Parameter and Contact Force Estimation of Planar Rigid-Bodies Undergoing Frictional Contact

Nima Fazeli, Roman Kolbert, Russ Tedrake, and Alberto Rodriguez

April 6, 2017

Abstract

This paper addresses the identification of the inertial parameters and the contact forces associated with objects making and breaking frictional contact with the environment. Our goal is to explore under what conditions, and to what degree, the observation of physical interaction, in the form of motions and/or applied external forces, is indicative of the underlying dynamics that governs it. In this study we consider the cases of passive interaction, where an object free-falls under gravity, and active interaction, where known external perturbations act on an object at contact. We assume that both object and environment are planar and rigid, and exploit the well-known complementarity formulation for contact resolution to establish a constrained optimization-based problem to estimate inertial parameters and contact forces. We also show that when contact modes are known, or guessed, the formulation provides a closed-form relationship between inertial parameters, contact forces, and observed motions, that turns into a least squares problem.

Consistent with intuition, the analysis indicates that without the application of known external forces, the identifiable set of parameters remains coupled, i.e., the ratio of mass moment of inertia to mass and the ratio of contact forces to the mass. Interestingly the analysis also shows that known external forces can lead to decoupling and identifiability of mass, mass moment of inertia, and normal and tangential contact forces. We evaluate the proposed algorithms both in simulation and with real experiments for the cases of a free falling square, ellipse, and rimless wheel interacting with the ground, as well as a disk interacting with a manipulator.

1 Introduction

Autonomous manipulation in an uncertain environment can benefit from an explicit understanding of contact. The *a priori* models of objects and environment that robots rely on are inevitably deficient or defective: In some cases it is not cost-effective to build accurate models; in others the complex and transforming nature of nature makes it impossible. This understanding of contact is often made implicit in the design of a manipulator. We deal with uncertainty

To appear in The International Journal of Robotics Research 2017. This paper is a revision of [13] appearing in the proceedings of the 2015 International Symposium on Robotics Research (ISRR).

Nima Fazeli, Roman Kolbert and Alberto Rodriguez are with the Department of Mechanical Engineering at the Massachusetts Institute of Technology, 77 Massachusetts Ave, Cambridge, MA 02139, <nfazeli, rkolbert, albertor@mit.edu>.

Russ Tedrake is with the Computer Science and Artificial Intelligence Laboratory at the Massachusetts Institute of Technology, 77 Massachusetts Ave, Cambridge, MA 02139, <russt@csail.mit.edu>.

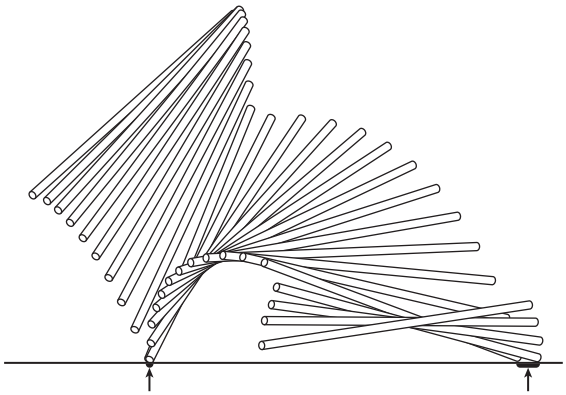

Figure 1: Is the trajectory of the rod in the figure indicative of the dynamic system that governs its motion? Note the two key events: When the left end of the rod makes contact and sticks to the ground, and the subsequent contact when the right end of the rod contacts the ground and slides. Stewart and Trinkle [30] used the example of a falling rod to introduce a time-stepping complementarity scheme for contact resolution that has become one of the standard techniques for simulating frictional contact. In this paper we look at the same formulation and similar examples from the perspective of identification.

by carefully choosing materials and geometries. However, when we want to monitor or actively control the execution of a manipulation task, an explicit understanding of the algebra between motions, forces, and inertias at contact is principal.

We are inspired by humans' unconscious but effective biases that make sense of contact to understand their environment. It only takes us a small push to a cup of coffee to estimate how full it is, and a quick glance to a bouncing ball to gauge its stiffness. Similarly, this work aims for robots to harness known laws of physical interaction to make sense of observed motions and/or forces, and as a result gain a better understanding of their environment and themselves.

In particular, in this study we explore the identifiability of inertial parameters and contact forces associated with planar frictional contact interactions. We exploit the linear complementarity formulation (LCP) of contact resolution (Stewart and Trinkle [30], Anitescu and Potra [1]) to relate inertial parameters, contact forces, and observed motions. Section 3.1 reviews in detail the structure of an LCP problem and describes the mathematical framework necessary to outline the identifiability analysis.

What can we say about an object from observing its motions and/or forces? One specific type of system we consider is a single planar rigid body undergoing impact after a period of free fall, as in Figure 1. The trajectory of the rod is a ballistic motion following the dynamics of free fall, which are not too informative. The relevant events are when the left end of the rod makes contact and "sticks" to the ground, and when the opposite end makes contact and "slides" on the ground. The key challenge, and focus of this paper, is in finding a formulation suitable for system identification, that can handle the complexity of contact dynamics with unknown and intermittent reaction forces due to frictional contact. Such a formulation provides the basis of an approach for identification in a broader set of contact interactions.

Our main contribution is an analysis of the question of the identifiability of the mass, the moment of inertia, and contact forces from kinematic observations of frictional contact

interactions. Section 4 details that analysis both for cases when contacts stick or slip, as well as when known external forces are applied during contact. In this paper we use a batch approach to system identification, that estimates the inertial parameters and contact forces that explain a window of observations. A potential benefit over more traditional calibration methods for parameter fitting, is that equivalent on-line techniques are well understood and readily available.

Section 5 and Section 6 demonstrate the validity of the approach through simulated and real experiments on single contact events, with a planar square, an ellipse, and a rimless wheel free-falling against a flat ground, and with the multiple-contact scenario of a manipulator interacting with a disk rolling on the ground.

2 Background & Motivation

System identification studies the problem of fitting a model (i.e., inertial parameters) to a series of inputs (i.e., forces and torques) and responses (i.e., displacements/velocities/accelerations) of a dynamic system. The basic idea behind system identification is that, although the response of a dynamic system tends to be complex, the governing dynamics are often linear in a set of observable parameters. For example, while $\sum \boldsymbol{f} = m \cdot \boldsymbol{a}$ can lead to complex trajectories, forces and accelerations are still linearly related by the mass m. In unconstrained dynamic systems, this allows closed-form least-squares formulations for the estimation of those parameters.

System identification determines what parameters, or combinations of parameters, are instrumental to a particular dynamic system, what observations are informative, and how to excite the system to trigger those observations, ultimately yielding estimates of the parameters. This idea has been applied in robotics to the identification of serial and parallel link manipulators [14, 17], and to identify inertial parameters sufficient for control purposes [29] among others.

In robotic manipulation, we often rely on dynamic models of impact and frictional interaction by assuming known masses, inertias, and coefficients of friction or restitution. For example many algorithms for contact-aware state estimation (Erdmann [12], Atkeson [3], Koval et al. [20], Zhang and Trinkle [36], Yu et al. [34]), use a dynamic model to filter noisy observations of state. Zhang et al. [37] studies the problem of simultaneously estimating state and inertial and frictional parameters in a planar pushing task. Our work characterizes what parameters can actually be estimated from the type of interaction and the available information. Ayusawa et al. [4] exploit the particularities of floating base robots to simplify the estimation of their inertial parameters. This work focuses on dealing with the issues that originate from the hybridness of making and breaking contact.

Close to our work, Kolev and Todorov [19] develop a similar approach to estimating inertial parameters, based on a physics engine with smoothed contact dynamics, leading to computationally efficient algorithms. More recently, in the context of a planar pushing task, Zhou et al. [38] propose to constrain the search for dynamic models to a convex polynomial relationship between forces and motions. The assumption, motivated by the principle of maximal dissipation and the concept of limit surface (Goyal et al. [15]), yields a data-efficient algorithm.

Algorithms for planning and control of dynamic manipulation through contact (Lynch and Mason [22], Platt and Kaelbling [25], Posa et al. [26], Chavan Dafle and Rodriguez [8], Hogan and Rodriguez [16]) also rely heavily on known dynamic parameters to make prediction

for given control inputs. Dynamic models are also widely used for fault detection and task monitoring, although to a lesser degree within the context of frictional contact. Willsky [33] provides an early review of methods to detect and diagnose changes in the evolution of a system from its expected behavior, where the expected behavior can be specified as following a particular parametrized dynamic model (Barai and Pandey [5], Salawu [28], De Luca and Mattone [10]) or data-driven model (Tax et al. [32], Rodriguez et al. [27]). Recently, Manuelli and Tedrake [23] propose to use a particle filter based scheme to estimate and localize external contacts to explain unexpected internal torques in a floating base mechanism like a humanoid. In all these cases, system identification has the potential to provide a formal approach to extract estimates of system parameters and contact forces from observations of rigid-body contact interactions.

The main design choice in our approach is the selection of a time-stepping Linear Complementarity Problem (LCP) scheme for the resolution of forces and accelerations (or rather impulses and velocities) during frictional contact. Why LCP? Brogliato et al. [7] identifies 3 classes of methods for rigid body simulation:

i. *Penalty methods* approximate contact interactions by allowing interpenetration of bodies and generating forces proportional to the amount of penetration, yielding smooth yet stiff systems that can be solved with integration methods. These methods yield computationally favorable solutions at the cost of realism.

ii. *Event-driven methods* rely on a listing, resolution, and selection of all possible contact/impact events. They typically require some knowledge of contact time which may be difficult to predict *a priori* for complicated multi-body systems.

iii. *Time-stepping methods* integrate the equations of motion during a finite time interval. Should a contact (or multiple) be detected during the interval, the algorithm resolves the collisions and continues to integrate the equations of motion.

The time-stepping approach, in conjunction with the velocity-impulse resolution of contact, which results in a Complementarity Problem (CP), has been advocated by Stewart and Trinkle [30] and Anitescu and Potra [2] among others, and has been shown to be robust to phenomena such as Painleve's problem [31], and to always yield a solution, with linear approximations of the friction cone. Specially interesting for this work, LCP, or CP in general, provides a unique consistent formulation over different contact modalities, i.e., contact vs. separation and sticking vs. slipping.

3 Complementarity Problems for Collision Resolution

The standard approach to resolve motion in unconstrained dynamic systems follows an iterative integration scheme:

$$\text{Current state} \longrightarrow \begin{array}{c}\text{Compute resultant}\\ \text{of applied forces}\end{array} \longrightarrow \begin{array}{c}\text{Integrate forward}\\ \text{to next state}\end{array}$$

A key difficulty in dealing with the constraints induced by rigid body contact dynamics, as in many constrained dynamical systems, is that it breaks this approach. From an algebraic perspective, forces and states must be consistent with the constraints, which complicates their

resolution. From a mechanical perspective, the motion of the system depends on the resultant of applied contact forces, while these applied contact forces (friction and contact normal) also depend on the motion of the system. Normal forces are only present if the system wants to move into contact. Equally, tangential friction forces depend on the relative motion at contact. For example, at a sliding point contact the direction of friction opposes the direction of sliding. This direction, however, is determined by the resultant of forces, including friction. As a consequence, both contact forces and resulting motions must be determined (searched for) simultaneously, instead of sequentially.

Penalty methods, by approximating contact forces as a measure of interpenetration, effectively can turn contact resolution back into the iterative integration scheme above. Methods that rely on contact enumeration search the space of motions and forces by decomposing all possible types of contact configurations each yielding a different model of contact forces.

This section reviews the complementarity formulation for contact resolution, a formulation that yields a consistent set of equations of the dynamics and constraints of contact, at the cost of increased algebraic complexity. The derivations in this section draw from Stewart and Trinkle [30] and Stewart [31], to which we refer the reader to for further detail.

3.1 A Linear Complementarity Problem

A general (i.e. nonlinear) complementarity problem is defined as:

$$\begin{aligned} \text{Find} \quad & \boldsymbol{z} && \\ \text{s.t.} \quad & \boldsymbol{z} && \geq \mathbf{0} \\ & \boldsymbol{g}(\boldsymbol{z}) && \geq \mathbf{0} \\ & \boldsymbol{z} \cdot \boldsymbol{g}(\boldsymbol{z}) && = \mathbf{0} \end{aligned} \tag{1}$$

The basic idea behind a complementarity problem is to encode two mutually exclusive conditions on $\boldsymbol{z}$. In the simple formulation above, we need to find a vector $\boldsymbol{z}$ that satisfies the two conditions $\boldsymbol{z} \geq \mathbf{0}$ and $\boldsymbol{g}(\boldsymbol{z}) \geq \mathbf{0}$, these being exclusive $\boldsymbol{z} \cdot \boldsymbol{g}(\boldsymbol{z}) = \mathbf{0}$, i.e., at least one of them must be $\mathbf{0}$. We see this often written in compact form as $\mathbf{0} \leq \boldsymbol{z} \perp g(\boldsymbol{z}) \geq \mathbf{0}$.

A linear complementarity problem (LCP) is formed when the constraint function g is linear $g(\boldsymbol{z}) = \boldsymbol{\Lambda}\boldsymbol{z} + \boldsymbol{b}$. Since their development in the 1960s [9], these formulations have found a wide application range. The complementarity conditions in Equation 1 arise naturally when setting up Lagrange multipliers for optimization problems with inequality constraints, and is a classical problem in optimization theory. In 1996 Pang and Trinkle [24] presented an algorithm based on LCP and an approximated version of Coulomb's frictional law to predict the instantaneous acceleration of a system of rigid bodies undergoing frictional contact. In this context, complementarity naturally encodes constraints such as the exclusivity between the magnitude of a contact force and the distance to contact (at all times one of them has to be zero), or between the magnitude of the sliding velocity at contact and the magnitude of the frictional force (either the sliding velocity is zero, or the frictional force has to reach the maximum determined by Coulomb's law). Provided algorithms exist to efficiently solve LCP problems, the formulation allows us to search the space of motions and forces without having to enumerate contact modes.

The equation of motion resulting from force balance for a single frictional contact can be

written as:

$$\boldsymbol{M}(\boldsymbol{q})\frac{d\boldsymbol{v}}{dt} + \boldsymbol{C}(\boldsymbol{q},\boldsymbol{v})\boldsymbol{v} = \boldsymbol{g}(\boldsymbol{q}) + \boldsymbol{f}_{\text{ext}}(\boldsymbol{q}) + \boldsymbol{J}_n^T(\boldsymbol{q})c_n + \boldsymbol{J}_t^T(\boldsymbol{q})\boldsymbol{c}_t \tag{2}$$

where $\boldsymbol{q}$ and $\boldsymbol{v}$ are respectively the joint configurations and velocities. The left side encodes the motion of the system where:

- $\boldsymbol{M}(\boldsymbol{q})$ is the (positive-definite) inertia matrix defined in joint space.
- $\boldsymbol{C}(\boldsymbol{q},\boldsymbol{v})\boldsymbol{v}$ represents the centrifugal and Coriolis accelerations.

and the right-hand side is the resultant of all applied forces:

- $\boldsymbol{g}(\boldsymbol{q})$ is the resultant of all conservative forces (only dependent on configuration). In this paper we only consider gravity, but it can also incorporate forces due to the deformation of non-rigid bodies.
- $\boldsymbol{f}_{\text{ext}}(\boldsymbol{q})$ is the resultant of all generalized external non-conservative forces, excluding contact.
- $\boldsymbol{J}_n^T(\boldsymbol{q})c_n$ is the contact normal force in an inertial reference frame, where c_n is its magnitude. $\boldsymbol{J}_n^T(\boldsymbol{q}) = \nabla\phi_n(\boldsymbol{q})^T$ is the gradient of a scalar "distance-to-contact" function $\phi_n(\boldsymbol{q})$ that determines the boundary between no contact ($\phi_n(\boldsymbol{q}) > 0$) and penetration ($\phi_n(\boldsymbol{q}) < 0$). Evaluated at contact ($\phi_n(\boldsymbol{q}) = 0$), it gives the outward normal to the contact surface in an inertial reference frame.
- $\boldsymbol{J}_t^T(\boldsymbol{q})\boldsymbol{c}_t$ is the contact frictional force in an inertial reference frame, where $\boldsymbol{c}_t$ is a magnitude along each basis vector in $\boldsymbol{J}_t^T(\boldsymbol{q})$. The columns of $\boldsymbol{J}_t^T(\boldsymbol{q})$ form a linear span of the tangent space at contact. Note that the combination of the columns in $\boldsymbol{J}_t^T(\boldsymbol{q})$ with $\boldsymbol{J}_n^T(\boldsymbol{q})$ gives a full linear basis, or reference frame, at a contact.

Equation 2 is an unconstrained dynamic system with forces $\boldsymbol{c}_t$, c_n as inputs. We can change the pose $\boldsymbol{q}$ of an object by choosing the geometry of contact $\boldsymbol{J}_n(\boldsymbol{q}), \boldsymbol{J}_t(\boldsymbol{q})$ and by controlling the magnitude of the contact forces $\boldsymbol{c}_t$, c_n. In this context, classical system identification would provide a well-understood process to estimate problem parameters and forces, leading to a least-squares problem formulation [21], as we will see in examples in Section 5.

Unfortunately, without making assumptions about the interaction mode, $\boldsymbol{c}_t$ and c_n are constrained, and depend both on each other and on the states $(\boldsymbol{q},\boldsymbol{v})$. They are constrained by motion principles and by frictional laws. First, the magnitude of the normal force c_n should always be positive, and different than zero only at contact, $\phi_n(\boldsymbol{q}) = 0$. At the same time, the distance to contact should always be positive, and zero only when in contact. We can write both conditions compactly as the complementarity constraint $0 \leq \phi_n(\boldsymbol{q}) \perp c_n \geq 0$. Second, the motion at contact and the tangential frictional force $\boldsymbol{J}_t(\boldsymbol{q})\boldsymbol{c}_t$ are related by the maximum power inequality [1]. This states that during contact the selection of motion and frictional forces is resolved to maximize power dissipation, which we have seen experimentally to be a good approximation in tasks such as pushing (Yu et al. [35]) or prehensile pushing (Kolbert et al. [18]):

$$\min_{\boldsymbol{c}_t} \boldsymbol{v} \cdot \boldsymbol{J}_t^T(\boldsymbol{q})\boldsymbol{c}_t \qquad \text{s.t. } (c_n, \boldsymbol{c}_t) \text{ satisfy friction law} \tag{3}$$

In practice, and in simple cases such as point contacts, contact resolution searches for the components of $\boldsymbol{c}_t$ such that the frictional force $\boldsymbol{J}_t(\boldsymbol{q})\boldsymbol{c}_t$ maximally opposes the instantaneous

sliding velocity $\boldsymbol{v}$ from within a valid domain of contact forces. That domain is specified by a frictional law, which constrains the normal and tangential components of the contact force, and is commonly represented by an inequality constraint $\psi(\boldsymbol{c}_t) \leq \mu c_n$, with μ as the scalar coefficient of friction and $\psi(\cdot)$ a scalar function. In this case Equation 3 looks like:

$$\min_{\boldsymbol{c}_t} \boldsymbol{v} \cdot \boldsymbol{J}_t^T(\boldsymbol{q})\boldsymbol{c}_t \qquad \text{s.t. } \psi(\boldsymbol{c}_t) \leq \mu c_n \tag{4}$$

Note that Coulomb's law is the special case when $\psi(\boldsymbol{c}_t) = ||\boldsymbol{c}_t||_2$, i.e., all contact forces must lie inside the friction cone $FC(\boldsymbol{q}) = \{\boldsymbol{J}_n^T(\boldsymbol{q})c_n + \boldsymbol{J}_t^T(\boldsymbol{q})\boldsymbol{c}_t \text{ s.t. } ||\boldsymbol{c}_t||_2 \leq \mu c_n\}$. We can incorporate this constraint in the minimization in Equation 4 through a Lagrange multiplier λ, where we minimize now $h(\boldsymbol{c}_t, \lambda) = \boldsymbol{v}^T \cdot \boldsymbol{J}_t^T(\boldsymbol{q})\boldsymbol{c}_t - \lambda(\mu c_n - \psi(\boldsymbol{c}_t))$ with respect to both $\boldsymbol{c}_t$ and λ. The conditions for optimality for a minimization problem with inequality constraints are known as the Karush-Kuhn-Tucker conditions [6]:

$$\begin{aligned} \frac{\partial h}{\partial \boldsymbol{c}_t} = \boldsymbol{J}_t(\boldsymbol{q})\boldsymbol{v} + \lambda\frac{\partial \psi(\boldsymbol{c}_t)}{\partial \boldsymbol{c}_t} &= 0 \\ \lambda &\geq 0 \\ \mu c_n - \psi(\boldsymbol{c}_t) &\geq 0 \\ \lambda \cdot (\mu c_n - \psi(\boldsymbol{c}_t)) &= 0 \end{aligned} \tag{5}$$

which are the origin of the algebraic expression of the complementarity conditions.

We can then complete the complementarity formulation for contact resolution (for one point contact) as:

$$\begin{aligned} \frac{d\boldsymbol{q}}{dt} &= \boldsymbol{v} \\ \boldsymbol{M}(\boldsymbol{q})\frac{d\boldsymbol{v}}{dt} + \boldsymbol{C}(\boldsymbol{q}, \boldsymbol{v})\boldsymbol{v} &= \boldsymbol{g}(\boldsymbol{q}) + \boldsymbol{f}_{\text{ext}}(t) + \boldsymbol{J}_n^T(\boldsymbol{q})c_n + \boldsymbol{J}_t^T(\boldsymbol{q})\boldsymbol{c}_t \\ \text{Subject to:} \qquad 0 &= \boldsymbol{J}_t(\boldsymbol{q})\boldsymbol{v} + \lambda\frac{\partial \psi(\boldsymbol{c}_t)}{\partial \boldsymbol{c}_t} \\ 0 &\leq \phi_n(\boldsymbol{q}) \perp c_n \geq 0 \\ 0 &\leq \lambda \perp (\mu c_n - \psi(\boldsymbol{c}_t)) \geq 0 \end{aligned} \tag{6}$$

It is possible to add an extra constraint $\boldsymbol{J}_n(\boldsymbol{q}) \cdot (\boldsymbol{v}^+ + \epsilon\boldsymbol{v}) = 0$ when $\phi_n(\boldsymbol{q}) = 0$ to model the elasticity of the contact, where ϵ denotes the coefficient of restitution and $\boldsymbol{v}^+$ the post contact velocity. For the perfectly inelastic case, $\epsilon = 0$, the constraint turns into $\boldsymbol{J}_n(\boldsymbol{q})\boldsymbol{v}^+ = 0$ when $\phi_n(\boldsymbol{q}) = 0$ which simply zeroes the normal component of the velocity after contact.

The optimization problem in Equation 6 is nonlinear, due to the friction surface function ψ. For computational reasons, it is common to linearize the friction cone by approximating it as a polyhedral convex cone. We construct it by using a finer discretization of the tangent space at contact with a set of vector generators $\{d_i(\boldsymbol{q})\}_{i=1\ldots m}$ that positively span it. It will be convenient to chose these vectors equispaced and paired to each other $d_i = -d_j$ as in Stewart and Trinkle [30]. We then stack this larger set of generators in the same matrix $\boldsymbol{J}_t^T(\boldsymbol{q})$ with which we can express any frictional force as a positive linear combination $\boldsymbol{J}_t^T(\boldsymbol{q})\boldsymbol{c}_t$ with $\boldsymbol{c}_t \geq \boldsymbol{0}$, subject to the approximated Coulomb's frictional law $\psi(\boldsymbol{c}_t) = \sum_{i=1}^m c_{t,i} \leq \mu c_n$ where $\boldsymbol{c}_t = (c_{t,1} \ldots c_{t,m})$, and under the complementarity condition that $\boldsymbol{c}_t \geq \boldsymbol{0}$. Applying this

approximation we can write:

$$\frac{d\boldsymbol{q}}{dt} = \boldsymbol{v} \tag{7}$$

$$\begin{aligned}
\boldsymbol{M}(\boldsymbol{q})\frac{d\boldsymbol{v}}{dt} + \boldsymbol{C}(\boldsymbol{q},\boldsymbol{v})\boldsymbol{v} &= \boldsymbol{g}(\boldsymbol{q}) + \boldsymbol{f}_{\text{ext}}(t) + \boldsymbol{J}_n^T(\boldsymbol{q})c_n + \boldsymbol{J}_t^T(\boldsymbol{q})\boldsymbol{c}_t \\
\text{Subject to:} \quad & 0 \leq \boldsymbol{c}_t \perp \boldsymbol{J}_t(\boldsymbol{q})\boldsymbol{v} + \lambda\boldsymbol{e} \geq 0 \\
& 0 \leq \phi_n(\boldsymbol{q}) \perp c_n \geq 0 \\
& 0 \leq \lambda \perp (\mu c_n - \sum_{i=1}^{m} c_{t,i}) \geq 0
\end{aligned}$$

where $\boldsymbol{e}$ is a vector of all ones, that originates when differentiating $\psi(\boldsymbol{c}_t) = \sum_{i=1}^{m} c_{t,i}$ with respect to $\boldsymbol{c}_t$. In the rest of the paper we will focus on the specific case of planar contacts, i.e., at every contact there are only two generators $m = 2$ of the polyhedral friction cone spanning the tangent space, both opposite to each other. Note that in practice, this is equivalent to using the true Coulomb friction cone, but it better generalizes for higher dimensions.

3.2 A Time-Stepping Approach

Shortly after Pang and Trinkle [24] introduced the instantaneous LCP formulation for contact resolution in the space of forces and accelerations, Stewart and Trinkle [30] proposed a time-stepping formulation in the space of impulses and velocities which added stability and effectiveness for forward simulation. The resulting equations of motion and constraints are based on a discretization of Equation 7 and follow from Stewart [31]. For the particular case of one contact in the plane we can write them as:

$$\boldsymbol{q}^{k+1} - \boldsymbol{q}^k = h\boldsymbol{v}^{k+1} \tag{8}$$

$$\begin{aligned}
\boldsymbol{M}(\boldsymbol{q}^{k+1})\left(\boldsymbol{v}^{k+1} - \boldsymbol{v}^k\right) + \boldsymbol{C}(\boldsymbol{q}^{k+1},\boldsymbol{v}^{k+1})\boldsymbol{v}^{k+1} &= \boldsymbol{g}(\boldsymbol{q}^{k+1}) + \boldsymbol{f}_{\text{ext}}^k + \\
&\quad + \boldsymbol{J}_n^T(\boldsymbol{q}^{k+1})c_n + \boldsymbol{J}_t^T(\boldsymbol{q}^{k+1})\boldsymbol{c}_t \\
0 \leq \boldsymbol{c}_t \perp \boldsymbol{J}_t(\boldsymbol{q}^{k+1})\boldsymbol{v}^{k+1} + \lambda\boldsymbol{e} &\geq 0 \\
0 \leq \phi_n(\boldsymbol{q}^k) \perp c_n &\geq 0 \\
0 \leq \lambda \perp \mu c_n - (c_{t,1} + c_{t,2}) &\geq 0
\end{aligned}$$

where superscripts k and $k+1$ denote discretized time. Note that the first constraint is a vector with one complementarity constraint for every generator of the contact tangent space $\boldsymbol{J}_t$, all sharing the same Lagrange multiplier λ.

The particular time-stepping method used in Equation 8 is based on an implicit Euler integration scheme, but can be adapted to other methods. To simulate forward a single-contact rigid-body frictional interaction between two rigid bodies, we need to solve the set of equations and complementarity constraints in Equation 8. To do so, we search for the velocity of the object $\boldsymbol{v}^{k+1}$ and consistent values of the contact forces $c_n, \boldsymbol{c}_{t,i}$ that step the system from instant k to instant $k+1$.

The search is also over the values of the extra variables introduced to formulate the complementarity constraints, ϕ and λ, which determine the contact mode, i.e., contact vs. no-contact and sticking vs. slipping. We will exploit this in the following sections for the purpose of

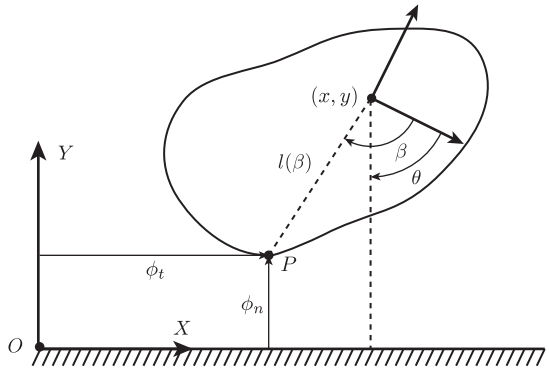

Figure 2: Distance to contact. For a planar object falling on a horizontal surface aligned with axis X, we consider the distances ϕ_n and ϕ_t between the closest point to the ground P and the origin O of a fixed reference frame. Following Equation 9, the coordinates of point P are given by the configuration of the object $\boldsymbol{q} = (x, y, \theta)$, the angle β, and the distance $l(\beta)$.

parameter and force estimation. We emphasize that if the contact mode is known or assumed, there is no need to solve the LCP. In that case, impulses during impact and velocities post-impact can be solved strictly as functions of states and external influences pre-impact. We will use this in Section 4.3 and Section 4.4 to find closed-form relations between impulses, velocities, and inertial parameters.

3.3 Regarding the Distance Function $\phi_n(\cdot)$

The function $\phi_n(\cdot)$ measures the minimum distance between the boundaries of two interacting rigid bodies (or a body and the environment). The particular form of that function depends on the geometry of the problem.

Consider the example in Figure 2 of a rigid object falling under gravity on a fixed ground. The function $\Phi(\boldsymbol{q}) = (\phi_n, \phi_t)$ parametrizes the position of point P (closest to the ground) in an inertial reference frame. The object is in free space if $\phi_n > 0$, in contact if $\phi_n = 0$, and in penetration if $\phi_n < 0$. We can write Φ as:

$$\Phi = \begin{bmatrix} \phi_n \\ \phi_t \end{bmatrix} = \begin{bmatrix} y - l(\beta)\cos(\beta - \theta) \\ x - l(\beta)\sin(\beta - \theta) \end{bmatrix} \tag{9}$$

where β parametrizes the contact point P in an object-fixed reference frame, and $l(\cdot)$ parametrizes the object boundary. In an inertial reference frame, the closest point P is also a function of the orientation of the object θ. the geometry of contact is then given by the function $\beta(\theta)$ defined in the interval $0 \leq \beta(\theta) < 2\pi$.

The equation of motion derived in the previous section requires the Jacobian of the distance function in Equation 9:

$$\boldsymbol{J} = \frac{\partial \Phi}{\partial q} = \begin{bmatrix} \boldsymbol{J}_n \\ \boldsymbol{J}_t \end{bmatrix} = \begin{bmatrix} 0 & 1 & J_y(\theta) \\ 1 & 0 & J_x(\theta) \end{bmatrix} \tag{10}$$

with

$$J_y = -\frac{\partial \beta}{\partial \theta}\left(\frac{\partial l}{\partial \beta}\cos(\beta-\theta) - l\sin(\beta-\theta)\right) - l\sin(\beta-\theta)$$
$$J_x = -\frac{\partial \beta}{\partial \theta}\left(\frac{\partial l}{\partial \beta}\sin(\beta-\theta) + l\cos(\beta-\theta)\right) + l\cos(\beta-\theta)$$

where the rows of $\boldsymbol{J}$, or columns of $\boldsymbol{J}^T$, can be seen as a mapping projecting Cartesian contact forces in the local contact frame to generalized forces in a global inertial frame.

4 Identifiability Analysis

In this section we study the identifiability of inertial parameters (masses and inertias) and contact forces of rigid bodies making and breaking frictional contact with the environment. In Section 4.1 we will briefly review the key concepts of identifiability analysis and what it means for a parameter to be identifiable. The following subsections will discuss the application of this analysis to the problem of planar rigid body contact.

4.1 Key Concepts in Identifiability Analysis

System identification is a well developed field, with many excellent texts [21], which we make use of here. In its barest form, system identification seeks to answer two questions, i) what is the set of parameters from a dynamical system that we can hope to estimate (identifiability) given sufficient observations, and ii) how to estimate them (identification). In this paper we study a special class of systems in which the inputs and outputs are related through a linear set of parameters. This class of systems has been shown to include a large set of rigid body robotic systems [17].

To illustrate the principles of system identification, consider the following 1 D.O.F. dynamic system subject to a harmonic excitation with a known magnitude a and frequency ω (a.k.a. Duffing oscillator):

$$m\ddot{x} + c\dot{x} + k_1 x + k_2 x^3 = a\cos(\omega) \tag{11}$$

for which the parameter set $\boldsymbol{\theta} = [m, c, k_1, k_2]^T$ is unknown. We can relate observations of the input force (excitation) $a\cos(\omega)$ and states $(\ddot{x}, \dot{x}, x)$ to the unknown parameter set as:

$$\begin{bmatrix}\ddot{x} & \dot{x} & x & x^3\end{bmatrix} \cdot \boldsymbol{\theta} = a\cos(\omega) \tag{12}$$

or more generally,

$$\boldsymbol{Y}(\ddot{x}, \dot{x}, x) \cdot \boldsymbol{\theta} = \boldsymbol{f} \tag{13}$$

where $\boldsymbol{Y}$ is a non-linear function of the observed state, $\boldsymbol{\theta}$ is the parameter set, and $\boldsymbol{f}$ is the known input. Equation 13 has a linear regression form, and given N observations of $(\boldsymbol{Y}, \boldsymbol{f})$ with N larger than the dimension of $\boldsymbol{\theta}$, we will be able to estimate $\boldsymbol{\theta}$, assuming the matrix $\boldsymbol{Y}$ is sufficiently well conditioned. In this formulation, the identifiable set is $\boldsymbol{\theta}$ which can be estimated by solving a least squares problem. In this work, the inputs are contact reaction forces. This does not change the form of the identifiability problem, or the identifiable set,

rather it will affect our ability to generate informative trajectories, since we do not have direct control over those contact forces, which ultimately affects the structure of the matrix $\boldsymbol{Y}$, as further described in Section 7.3.

It is interesting to note that if we eliminate the excitation and apply initial conditions to the system then the linear regression formulation can be written as:

$$\begin{bmatrix} \dot{x} & x & x^3 \end{bmatrix} \hat{\boldsymbol{\theta}} = -\ddot{x} \tag{14}$$

where $\hat{\boldsymbol{\theta}} = [\frac{c}{m}, \frac{k_1}{m}, \frac{k_2}{m}]^T$. The parameters of the original system are now coupled to each other and not distinguishable, i.e. the identifiable set is lower dimensional.

In the discussion so far we have not considered constraints on the dynamics of the system. This is only the case when the contact mode is constant and known. The rest of this section is dedicated to the study of the identification problem for systems that make and break contact, in which we need to explicitly handle constraints and changing contact modes.

4.2 Parameter and Contact Force Estimation Through Contact

Identifiability analysis starts by writing the left-hand side of the dynamic equation of motion in Equation 8 in linear form $\boldsymbol{Y}(\boldsymbol{q}, \boldsymbol{v}, \dot{\boldsymbol{v}}) \cdot \boldsymbol{\theta}$, with the parameter vector $\boldsymbol{\theta}$ called the base inertial parameters. The structure of the base inertial parameters depends on the geometry of the problem, and dictates what can or cannot be identified or estimated. It is often the case that the parameters we want to estimate are coupled [21]. In this section we study the problem of determining and estimating the base inertial parameter set and contact forces with no *a priori* assumption on contact modes. In followup subsections we will make assumptions on the contact mode to show insights into how the identifiable set changes given the presence or absence of known excitation.

Recalling Equation 8 we can write the dynamic equation of motion between two time steps k and $k+1$ as:

$$\begin{aligned} \boldsymbol{q}^{k+1} - \boldsymbol{q}^k &= h\boldsymbol{v}^{k+1} \\ \boldsymbol{Y}(\boldsymbol{q}^{k+1}, \boldsymbol{v}^k, \boldsymbol{v}^{k+1}, h) \cdot \boldsymbol{\theta} &= \boldsymbol{f}_{\text{ext}}^k + \boldsymbol{J}_n^T(q^{k+1})c_n + \boldsymbol{J}_t^T(q^{k+1})\boldsymbol{c}_t \end{aligned} \tag{15}$$

subject to a set of constraints, where we note that we incorporated gravity $\boldsymbol{g}(\boldsymbol{q}^{k+1})$ on the left-hand side of the equation. For compactness of notation, we introduce the vectors:

$$\begin{aligned} \boldsymbol{J}_c^T(\boldsymbol{q}) &= \begin{bmatrix} \boldsymbol{J}_n^T(\boldsymbol{q}) & \boldsymbol{J}_t^T(\boldsymbol{q}) \end{bmatrix} \\ \boldsymbol{c}^T &= \begin{bmatrix} c_n & \boldsymbol{c}_t \end{bmatrix}^T \end{aligned} \tag{16}$$

where $\boldsymbol{J}_c^T(\boldsymbol{q})$ projects Cartesian space forces into joint space generalized forces. We can then rewrite Equation 15 as:

$$\begin{aligned} \boldsymbol{q}^{k+1} - \boldsymbol{q}^k &= h\boldsymbol{v}^{k+1} \\ \boldsymbol{Y}(\boldsymbol{q}^{k+1}, \boldsymbol{v}^k, \boldsymbol{v}^{k+1}, h)\boldsymbol{\theta} &= \boldsymbol{f}_{\text{ext}}^k + \boldsymbol{J}_c^T(\boldsymbol{q}^{k+1})\boldsymbol{c} \end{aligned} \tag{17}$$

We assume we have access to a time-limited window of noisy observations of the state of the system $\{\boldsymbol{q}^1 \dots \boldsymbol{q}^m\}$ and we are interested in estimating the values of the base parameters $\boldsymbol{\theta}$ and contact forces $\{\boldsymbol{c}^1 \dots \boldsymbol{c}^m\}$ that best explain that series of observations. Figure 3 illustrates

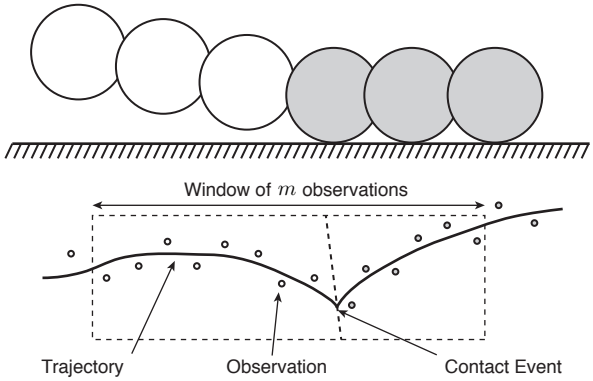

Figure 3: A disk transitions from free flight to rolling contact. The solid line denotes the true trajectory of the disk, and the dots denote observations corrupted by sensor noise. Given an observation window of length m we want to estimate the inertial parameters of the ball $\boldsymbol{\theta}$ and the contact forces $\{\boldsymbol{c}^1 \dots \boldsymbol{c}^m\}$ for the duration of the window.

an example problem where a disk comes into contact with a rigid surface. The true trajectory of the disk is shown with a solid line, and the noisy observations $\boldsymbol{q}^i$ are depicted with circles.

We use r to denote the dimension of the parameter space, $\boldsymbol{\theta} \in \mathbb{R}^r$. We use p to denote the number of generators in the linear approximation of the friction cone, so we can express the contact force with $p+1$ positive numbers, $\boldsymbol{c} \in (\mathbb{R}^+)^{p+1}$, one for the normal force and p for the tangent force. The total number of parameters we want to estimate is then $r + m(p+1)$, which for the planar examples in this paper becomes $r + 3m$.

In this section we use the example of a single planar body and a single point contact to illustrate the formulation. We will describe and estimate its base parameters, as well as the magnitude of the normal and friction forces c_n, c_1 and c_2. We find the most likely estimates of $\boldsymbol{\theta}$ and $\{\boldsymbol{c}^1 \dots \boldsymbol{c}^m\}$ by minimizing their fit to the time-stepped dynamic equation of motion and the series of constraints in Equation 8. The equations of motion must be satisfied in between any two sequential observations k and $k+1$, and the constraints must be satisfied at all m time-steps in the window. This takes the form of a nonlinear optimization problem, in a similar fashion to recent approaches for trajectory optimization through contact (Posa et al. [26]):

$$
\begin{aligned}
\min_{\boldsymbol{\theta}, \boldsymbol{c}^1 .. \boldsymbol{c}^m, \lambda} \quad & \left\| \boldsymbol{f}_{\text{ext}}^k - \left[\boldsymbol{Y}(\boldsymbol{q}^{k+1}, \boldsymbol{v}^k, \boldsymbol{v}^{k+1}, h) \quad - \boldsymbol{J}_c^T(\boldsymbol{q}^{k+1}) \right] \begin{bmatrix} \boldsymbol{\theta} \\ \boldsymbol{c}^{k+1} \end{bmatrix} \right\|_2 \\
\text{s.t:} \quad & 0 \le \boldsymbol{c}_t^{k+1} \perp \boldsymbol{J}_t(\boldsymbol{q}^{k+1}) \boldsymbol{v}^{k+1} + \lambda^{k+1} \boldsymbol{e} \ge 0 \quad \forall k = 1..m \\
& 0 \le \phi_n(q^k) \perp c_n^{k+1} \ge 0 \quad \forall k = 1..m \\
& 0 \le \lambda^{k+1} \perp \mu c_n^{k+1} - (c_{t,1}^{k+1} + c_{t,2}^{k+1}) \ge 0 \quad \forall k = 1..m
\end{aligned}
\tag{18}
$$

where we have one complementarity constraint modulated by the distance to contact $\phi_n(q^k)$, one complementarity constraint modulated by the magnitude of the relative velocity at contact λ^{k+1}, and two complementarity constraints, each modulated by the force along the corresponding generators of the contact tangent plane $c_{t,1}^k$ and $c_{t,2}^k$.

Note that the regressor matrix $\boldsymbol{Y}$ and the parameter vector $\boldsymbol{\theta}$, have been appended with the contact Jacobian and the contact forces respectively. The constraints resolve the contact mode

and enforce physically realizable values for the contact forces as well as the inertial parameters. We will see in following subsections that assuming we know exactly the mode of contact, we can neglect the constraints and get back to the unconstrained linear least squares formulation described in Section 4.1. Before, we list a few important observations regarding the nonlinear problem in Equation 18:

- We assume we can directly observe or estimate the applied external forces $\boldsymbol{f}_{\text{ext}}^k$, the kinematic matrix $\left[\boldsymbol{Y}(\boldsymbol{q}^{k+1}, \boldsymbol{v}^k, \boldsymbol{v}^{k+1}, h) \quad -\boldsymbol{J}_c^T(\boldsymbol{q}^{k+1})\right]$, the distance $\phi_n(\boldsymbol{q}^k)$, and the velocity at contact $\boldsymbol{J}_t(\boldsymbol{q}^{k+1})\boldsymbol{v}^{k+1}$. In practice, these are estimated by numerically differentiating observed states $\boldsymbol{q}^k$ and by assuming knowledge of the geometry of the object and the environment.

- If $\boldsymbol{f}_{\text{ext}}$ is sufficiently rich, and the system is in contact, then the identifiable set is the full vector $\boldsymbol{\theta}$ as well as all contact forces. The state dependant contact constraints do not affect the base inertial parameter set, they instead impose that the estimated contact forces and identified parameters are physically consistent. The contact forces affect the dynamics linearly and so can be folded into the linear parameter formulation discussed in Section 4.1. It is important to note that the identification is only effective if the external forces are informative enough to excite the complete spectrum of dynamics of the system considered (Section 7.3).

- In the case $\boldsymbol{f}_{\text{ext}} = \boldsymbol{0}$, i.e., there is no known external actuation on the system for the duration of the motion, Equation 18 becomes homogeneous, and the optimization reduces to a singular value problem. The contact forces cannot be found independently of the parameter vector $\boldsymbol{\theta}$ and only a ratio of the two can be found, as in the example discussed in Section 4.1.

- The gravitational force $\boldsymbol{g}(q^{k+1})$ does not yield additional information with respect to the identifiability of inertial parameters. This is because the gravitational term is linear in inertias, which are consequently proportional to accelerations. An intuitive example is a free falling object where $m \cdot \boldsymbol{g} = m \cdot \boldsymbol{a}$, observing its motion is not informative about its mass.

- When there is no contact, i.e., $\phi(\boldsymbol{q}) > 0$, all constraints are satisfied trivially, and the nonlinear optimization problem becomes again linear least squares regression over the parameter vector $\boldsymbol{\theta}$. This is the case for several seminal works on system identification applied to robotics [17, 29].

The optimization program in Equation 18 is formulated to deal with unknown contact modes, this is critical since in practice these modes are often not known beforehand. In the following subsections, we gain insight by focusing on a single rigid body making contact with a rigid flat surface and solve away the complementarity constraints for the cases of sliding (Section 4.3) and sticking contact (Section 4.4), both leading to the same set of identifiable parameters.

4.3 Parameter and Contact Force Estimation For a Sliding Contact

Here we assume that the system of interest is a single rigid body making contact with a flat surface and assume it is in sliding contact mode during the window of observation. This

breaks the hybridness of the dynamics of intermittent frictional contact, and will resolve the complementarity constraints. During sliding, these complementarity constraints become:

$$c_n^k > 0 \qquad \lambda^k > 0 \qquad \boldsymbol{c}_t^k > 0 \tag{19}$$

where $\boldsymbol{c}_t^k$ is $c_{t,1}^k$ or $c_{t,2}^k$, depending on whether the object is sliding to the right or the left.

The choice of contact mode turns the problem into an unconstrained optimization. Expanding Equation 18 with the general expressions in Equation 8, and rewriting the linear system with c_n, $\boldsymbol{c}_t$ and λ as variables, we obtain:

$$\begin{bmatrix} J_n^T M^{-1} J_n & J_n^T M^{-1} J_t & 0 \\ J_t^T M^{-1} J_n & J_t^T M^{-1} J_t & 1 \\ \mu & -1 & 0 \end{bmatrix} \begin{bmatrix} c_n^k \\ \boldsymbol{c}_t^k \\ \lambda^k \end{bmatrix} = - \begin{bmatrix} J_n^T b \\ J_t^T b \\ 0 \end{bmatrix} \tag{20}$$

where:

$$b = v^k + hM^{-1}(-G(q^k) - C(q^k, v^k) + F_{\text{ext}}^k)$$

Expressions for all other terms are provided in Appendix A. Solving the linear system of equations for c_n and $\boldsymbol{c}_t$ we can write:

$$c_n^k = m \frac{v_y^k + \theta^k J_y^k - hg + \frac{h}{m}(F_y^k + h\frac{m}{I} F_\theta)}{1 + \left(J_y^{k2} + \mu J_x^k J_y^k \right) \frac{m}{I}} = \frac{\boldsymbol{c}_t^k}{\mu} \tag{21}$$

which solves contact forces as functions of the inertial properties, geometry of contact, and kinematic measurements. We replace the expressions for normal and tangential contact forces back into the equations of motion, yielding:

$$\begin{bmatrix} v_x^{k+1} - v_x^k \\ v_y^{k+1} - v_y^k + hg \\ v_\theta^{k+1} - v_\theta^k \end{bmatrix} = \frac{v_y^k + v_\theta^k J_y^k - hg + \frac{h}{m}(F_y^k + h\frac{m}{I} F_\theta^k)}{1 + \left(J_y^{k2} + \mu J_x^k J_y^k \right) \frac{m}{I}} \begin{bmatrix} \mu \\ 1 \\ \frac{m}{I} \left(J_y^k + \mu J_x^k \right) \end{bmatrix} + h \begin{bmatrix} \frac{F_x^k}{m} \\ \frac{F_y^k}{m} \\ \frac{F_\theta^k}{I} \end{bmatrix} \tag{22}$$

Recalling from Section 4.1 in order to study the identifiability of the system making contact we need to manipulate this expression into a linear form in the unknown parameters. With some algebraic manipulation, we can write $\boldsymbol{Y} \cdot \boldsymbol{\theta} = \boldsymbol{f}$, with:

$$\boldsymbol{Y}(\boldsymbol{q}, \boldsymbol{v}, \boldsymbol{f}_{\text{ext}}) = \begin{bmatrix} \boldsymbol{y}_1(\boldsymbol{q}, \boldsymbol{v}) \\ \boldsymbol{y}_2(\boldsymbol{q}, \boldsymbol{v}, \boldsymbol{f}_{\text{ext}}) \\ \boldsymbol{y}_3(\boldsymbol{q}, \boldsymbol{v}, \boldsymbol{f}_{\text{ext}}) \\ \boldsymbol{y}_4(\boldsymbol{q}, \boldsymbol{v}, \boldsymbol{f}_{\text{ext}}) \end{bmatrix}^T$$

$$\boldsymbol{\theta} = \begin{bmatrix} \frac{m}{I} \\ \frac{1}{m} \\ \frac{1}{I} \\ \frac{m}{I^2} \end{bmatrix}$$

The complete expressions are provided in Appendix A. This linear mapping $\boldsymbol{f} = \boldsymbol{Y} \cdot \boldsymbol{\theta}$ in the base parameters $\boldsymbol{\theta} = \left[\frac{m}{I} \ \frac{1}{m} \ \frac{1}{I} \ \frac{m}{I^2}\right]^T$ indicates that this is indeed the identifiable set (Section 4.1), i.e. that provided we have sufficiently rich external excitation (Section 7.3), we can estimate m and I independently. To estimate these parameters we collect N data points of the states and external forces and solve a linear least squares optimization to evaluate the mass and inertia of the object then plug the values found back into Equation 21 to find the contact forces.

Note that $\boldsymbol{Y}$ depends both on the states and the external forces. The second, third, and fourth columns are linear functions of the external forces whereas the first column is function only of states. This implies that if there is no known external excitation during the contact then $\boldsymbol{y}_2(\cdot) = \boldsymbol{y}_3(\cdot) = \boldsymbol{y}_4(\cdot) = \boldsymbol{0}$ and only the first column of the $\boldsymbol{Y}$ matrix provides any information. Consequently we can only estimate the first element of $\boldsymbol{\theta}$, that is the ratio of the mass to the inertia $\frac{m}{I}$. Equation 21 then yields the ratio of the contact forces to mass $\frac{\boldsymbol{c}_t}{m}$ and $\frac{c_n}{m}$.

4.4 Parameter and Contact Force Estimation For a Sticking Contact

Analogous to the sliding case, during sticking contact, the complementarity constraints in Equation 18 become:

$$c_n^k > 0 \qquad \lambda^k = 0 \qquad \boldsymbol{c}_t^k > 0 \tag{23}$$

Expanding Equation 18 with the general expressions in Equation 8, and rewriting the linear system with c_n, $\boldsymbol{c}_t$ and λ as variables, we obtain:

$$\begin{bmatrix} J_n^T M^{-1} J_n & J_n^T M^{-1} J_t \\ J_t^T M^{-1} J_n & J_t^T M^{-1} J_t \end{bmatrix} \begin{bmatrix} c_n^k \\ \boldsymbol{c}_t^k \end{bmatrix} = - \begin{bmatrix} J_n^T b \\ J_t^T b \end{bmatrix} \tag{24}$$

Following the same strategy as in Section 4.3, we solve for c_n and $\boldsymbol{c}_t$:

$$\begin{aligned} \begin{bmatrix} c_n^k \\ \boldsymbol{c}_t^k \end{bmatrix} = & \frac{-m}{1 + \frac{m}{I}\left({J_y^k}^2 + {J_x^k}^2\right)} \begin{bmatrix} 1 + \frac{m}{I} {J_x^k}^2 & -\frac{m}{I} J_x^k J_y^k \\ -\frac{m}{I} J_x^k J_y^k & 1 + \frac{m}{I} {J_y^k}^2 \end{bmatrix} \cdot \\ & \cdot \begin{bmatrix} v_y^k - hg + v_\theta^k J_y^k + \frac{h}{m}(F_y^k + \frac{m}{I} F_\theta^k J_y^k) \\ v_x^k + v_\theta^k J_x^k + \frac{h}{m}(F_x^k + \frac{m}{I} F_\theta^k J_x^k) \end{bmatrix} \end{aligned} \tag{25}$$

We construct the linear mapping $\boldsymbol{Y} \cdot \boldsymbol{\theta} = \boldsymbol{f}$, by replacing the last expression into the equations of motion, yielding:

$$\boldsymbol{Y}(\boldsymbol{q}, \boldsymbol{v}, \boldsymbol{f}_{\text{ext}}) = \begin{bmatrix} \boldsymbol{y}_1(\boldsymbol{q}, \boldsymbol{v}) \\ \boldsymbol{y}_2(\boldsymbol{q}, \boldsymbol{v}, \boldsymbol{f}_{\text{ext}}) \\ \boldsymbol{y}_3(\boldsymbol{q}, \boldsymbol{v}, \boldsymbol{f}_{\text{ext}}) \\ \boldsymbol{y}_4(\boldsymbol{q}, \boldsymbol{v}, \boldsymbol{f}_{\text{ext}}) \end{bmatrix}^T$$

$$\boldsymbol{\theta} = \begin{bmatrix} \frac{m}{I} \\ \frac{1}{m} \\ \frac{1}{I} \\ \frac{m}{I^2} \end{bmatrix}$$

The detailed expressions for $\boldsymbol{Y}$ and $\boldsymbol{f}$ are in Appendix B. By a similar inspection as in the previous section, we conclude that the inertial parameters m and I are uniquely identifiable in

the presence of known external forces. We can then infer the value of the contact forces from Equation 25.

In the case external forces do not exist $\boldsymbol{y}_2(\cdot) = \boldsymbol{y}_3(\cdot) = \boldsymbol{y}_4(\cdot) = 0$, in which case only the ratio of mass to the angular moment of inertia $\frac{m}{I}$, and the ratio of contact forces to the mass $\frac{c_n}{m}$ and $\frac{c_t}{m}$ are identifiable, consistent with the results in the sliding mode.

5 Identification for Single Body Interactions

In this section we demonstrate the application of the formulation in Equation 18 to several examples, and show results with both simulated and experimental data. Section 5.1 describes the application of the approach to single body interactions, in particular we set the focus on objects falling under gravity. Section 5.2 describes three particular examples, an ellipse, a square, and a rimless wheel, and we conclude the section with simulated (Section 5.3) and experimental (Section 5.4) results.

5.1 Identification Formulation

Let $\boldsymbol{q} = (x, y, \theta)^T$ be the state of the rigid body and $\boldsymbol{v} = (v_x, v_y, v_\theta)^T$ its derivative. The state of the object is then described by the vector $(x, y, \theta, v_x, v_y, v_\theta)^T$. Consider a rigid body as in Figure 2 falling under gravity with no external actuation. Equation 18 can be written as:

$$\underset{\theta, \boldsymbol{c}_{1\ldots m}^k}{\text{minimize}} \left\| \begin{bmatrix} v_x^{k+1} - v_x^k \\ v_y^{k+1} - v_y^k \\ v_\theta^{k+1} - v_\theta^k \end{bmatrix} - h \left(\begin{bmatrix} 0 \\ -g \\ 0 \end{bmatrix} + \frac{c_n^{k+1}}{m} \begin{bmatrix} 0 \\ 1 \\ \frac{m}{I} J_y^k \end{bmatrix} + \frac{\boldsymbol{c}_t^{k+1}}{m} \begin{bmatrix} 1 \\ 0 \\ \frac{m}{I} J_x^k \end{bmatrix} \right) \right\|_2 \tag{26}$$

subject to the same set of complementarity constraints as in Equation 18. Since there is no external actuation, as discussed in the previous sections, the inertial parameters are coupled to the contact forces and disambiguation is not possible. This fact may not be immediately obvious from Equation 26 so we relate this formulation to the least squares formulation in Section 4.3 and Section 4.4 by assuming a contact mode and solving away the complementarity constraints to arrive at:

$$\begin{aligned} \min_{\theta_1} \quad & ||\boldsymbol{Y} \cdot \boldsymbol{\theta} - \boldsymbol{f}||_2 \\ \text{where:} \quad & \boldsymbol{f} = v_\theta^{k+1} - v_\theta^k \\ & \boldsymbol{Y} = (v_x^{k+1} - v_x^k) J_x^k - (v_y^{k+1} - v_y^k + hg) J_y^k \\ & \boldsymbol{\theta} = \frac{m}{I} \end{aligned} \tag{27}$$

where the vectors and matrices are now scalars and where only the ratio of mass to inertia is identifiable. The solution of Equation 27 yields an estimate of $\frac{m}{I}$. It is important to note that the constraints of the optimization exist but now have to be solved implicitly (external detection of contact events and transitions). If this is possible then the least squares approach can be applied when contact occurs and the the ratio of contact forces to mass can be estimated through a process of back substitution using the estimate of $\frac{m}{I}$. The results in subsequent sections rather use the formulation in Equation 26 with explicit complementarity constraints and make no assumption over the contact mode.

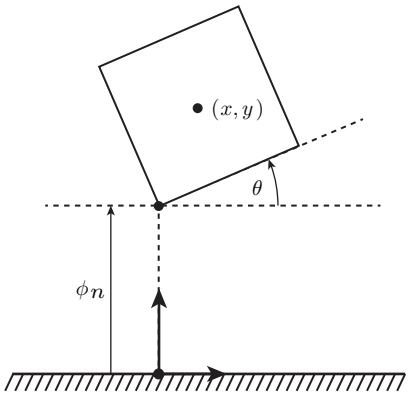

Figure 4: Parametrization of the contact geometry of a 2D square of side a.

5.2 Examples

So far we have not studied any particular contact geometry, and assumed that the contact Jacobian is a sufficient representation of the body. Yet algebraic expressions are required to compute that Jacobian as a function of the configuration of the object and its geometry. The following subsections show examples of analytical expressions for a square, ellipse, and rimless wheel which we will later use in simulated and real experiments.

5.2.1 2D Square

The square in Figure 4 models as a square with side length a, orientation θ, center of mass (x, y), mass m, and angular inertia I. The minimum distance from the square to the ground is the minimum of the vertical distances from all vertex:

$$\phi_n = \min\left(\begin{bmatrix} y - \frac{a}{\sqrt{2}}\cos(\pi/4 - \theta) \\ y - \frac{a}{\sqrt{2}}\cos(\pi/4 + \theta) \\ y + \frac{a}{\sqrt{2}}\cos(\pi/4 - \theta) \\ y + \frac{a}{\sqrt{2}}\cos(\pi/4 + \theta) \end{bmatrix} \right) \tag{28}$$

The contact Jacobian is derived from differentiating the distances in Equation 28 following the expressions in Equation 11. Assuming the first vertex is the lowest (with $\beta = \pi/4$ and $l = a/\sqrt{2}$), and since curvature does not play a role, i.e., $\frac{\partial \beta}{\partial \theta} = 0$, the expression of the normal and tangential Jacobians become:

$$\begin{aligned} \boldsymbol{J}_n(\boldsymbol{q}) &= \begin{bmatrix} 0 & 1 & -\frac{a}{\sqrt{2}}\sin(\pi/4 - \theta) \end{bmatrix} \\ \boldsymbol{J}_t(\boldsymbol{q}) &= \begin{bmatrix} 1 & 0 & \frac{a}{\sqrt{2}}\cos(\pi/4 - \theta) \end{bmatrix} \end{aligned} \tag{29}$$

which we could have also obtained by directly differentiating the distance function.

5.2.2 2D Ellipse

The ellipse in Figure 5 incorporates extra complexity due to its curvature. We will see that the resulting contact dynamics are sensitive to orientation, because small perturbations can produce large changes in contact location.

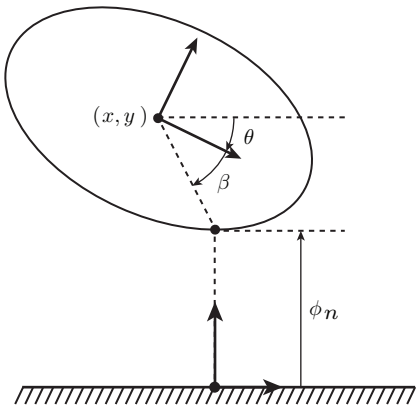

Figure 5: Parametrization of the contact geometry of an ellipse of major and minor principal radii a and b.

We parametrize the perimeter curve of the ellipse by angle β. Denote the major and minor radii of the ellipse with a and b, and its orientation with respect to a fixed reference frame by θ. The relationship between β to θ is given by:

$$\begin{aligned} \tan(\pi - \theta) &= -\frac{b}{a}\cot\beta \\ \frac{\partial\beta}{\partial\theta} &= -\frac{a}{b}\frac{1+\tan^2(\pi-\theta)}{1+\cot^2(\beta)} \end{aligned} \tag{30}$$

We now write the distance of any point on the perimeter of an ellipse from its center as:

$$\begin{aligned} l(\beta) &= \frac{ab}{\sqrt{b^2\cos^2\beta + a^2\sin^2\beta}} \\ \frac{\partial l}{\partial\theta} &= \frac{ab(b^2-a^2)\sin 2\beta}{2\sqrt{(b^2\cos^2\beta + a^2\sin^2\beta)^3}}\frac{\partial\beta}{\partial\theta} \end{aligned} \tag{31}$$

Which allows us to find the expression for $\partial l/\partial\theta$. By substituting in Equation 11 we can find an expression for the Jacobian.

5.2.3 Rimless Wheel

The rimless wheel is a classical example of a very simple passive walker. Its stability and gait cycles have been extensively studied. Here we demonstrate the application of parameter and contact force estimation approach to a rimless wheel as it "walks" down an incline. We make no assumption of sticking vs sliding motion. The formulation in Equation 18 applied to a rimless wheel becomes:

$$\min_{\theta, c_{1\ldots m}} \left\| \begin{bmatrix} v_x^{k+1} - v_x^k \\ v_y^{k+1} - v_y^k \\ v_\theta^{k+1} - v_\theta^k \end{bmatrix} - h \begin{bmatrix} \frac{1}{m} & 0 & 0 \\ 0 & \frac{1}{m} & 0 \\ 0 & 0 & \frac{1}{I} \end{bmatrix} \left(\begin{bmatrix} 0 \\ -mg \\ 0 \end{bmatrix} + \sum_{i=1}^{p} c_{n,i}^{k+1} \boldsymbol{J}_{n,i}^{k+1} + c_{t,i}^{k+1} \boldsymbol{J}_{t,i}^{k+1} \right) \right\|_2 \tag{32}$$

where we are now summing over the contact forces at all legs/spokes, since all legs can make contact with the ground. Note also the increase in complexity due to the fact that two simultaneous contact forces are possible.

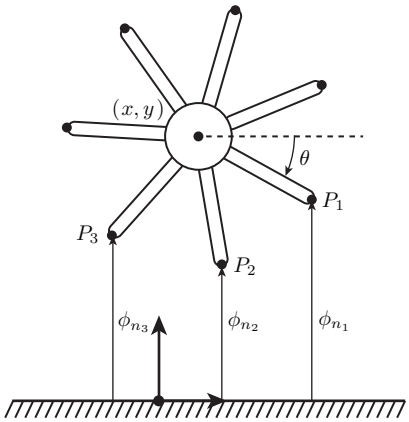

Figure 6: Parametrization of the contact geometry of an rimless wheel with six spokes. The figure shows the contact distance for 3 possible contact points. .

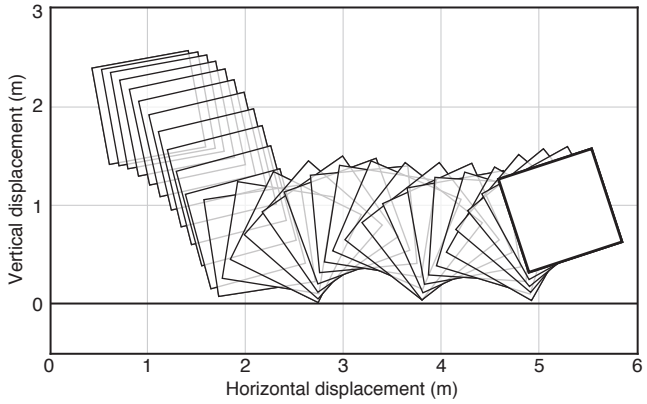

Figure 7: Example of a trace of an LCP simulation of a falling square.

5.3 Results from Simulated Data

In this section, we demonstrate the identification process with synthetic data for the square, ellipse, and rimless wheel. To do so, we simulate the time-stepping LCP formulation in Equation 7 and add Gaussian noise to state observations.

In the simulation we use a unit mass (kg), coefficient of restitution of 0.6 and a horizontal flat rigid surface with coefficient of friction 0.7. The ratio of mass m to angular inertia I moment of inertia for the square and ellipse are 6 (m^2) and 0.8 (m^2) respectively.

To generate data we gave the bodies a random set of initial positions and velocities and simulate their trajectory 100 times. Figure 7, Figure 8, and Figure 9 show traces of example trajectories for the square, ellipse, and rimless wheel respectively. For motivation, note in Figure 10 the dependence of the motion of the center of mass of the rimless wheel with its total mass, clearly indicating that, unlike in free fall, the trajectory through contact contains information regarding its inertial properties.

To test the robustness of the identification algorithm we add Gaussian noise o varying magnitude $\sim \mathcal{N}(0, \sigma^2)$ to the simulated data (both to configurations q and velocities v). We

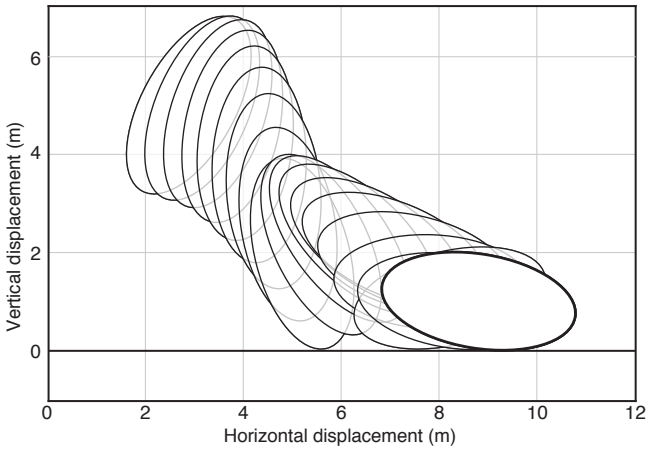

Figure 8: Example of a trace of an LCP simulation of a free-falling ellipse. The smoothness of the boundary of the ellipse leads to a more complex scenario, where the contact point can evolve while sticking (i.e., rolling) or sliding.

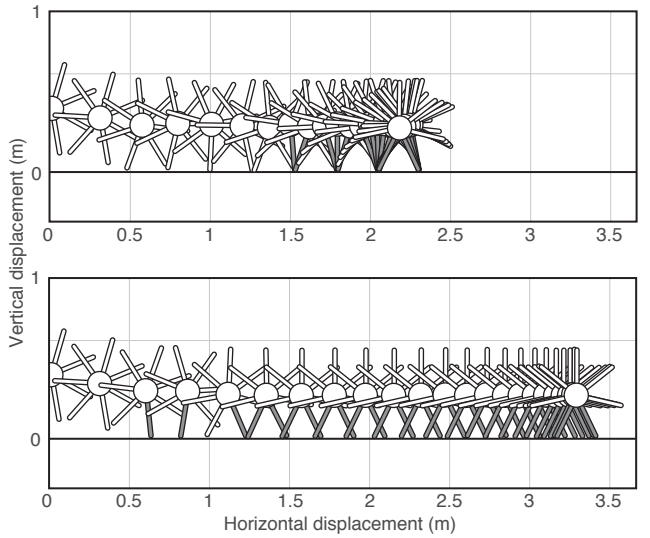

Figure 9: Example of a trace of an LCP simulation of a rimless wheel with (top) high friction and (bottom) low friction between wheel and ground. The dark spokes show the contacts that are (top) sticking and (bottom) slipping. The dynamics of the rimless wheel are very dependent on whether contacts slip or stick. As we have argued, this is a key difficulty in doing system identification.

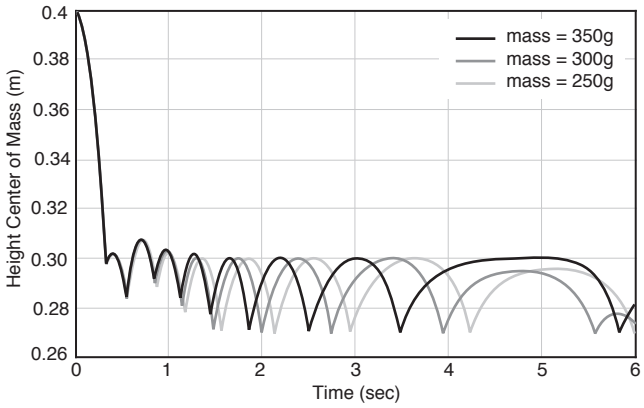

Figure 10: Dependence of the trajectory of the rimless wheel with its mass. Intuitively, the trajectory contains information of its inertial properties.

Table 1: Identification of $\frac{m}{I}$ from simulated data

Mean Error ± std.	Error (%)	S.N.R. (dB)
Square		
-0.02 ± 0.10 m^2	0.3	40
-0.12 ± 0.31 m^2	2.1	30
-0.66 ± 0.91 m^2	11.0	20
-3.49 ± 1.37 m^2	58.2	10
Ellipse		
-0.03 ± 0.10 m^2	0.3	40
-0.14 ± 0.44 m^2	2.3	30
-0.71 ± 0.82 m^2	11.7	20
-4.89 ± 1.94 m^2	80.4	10

then use the corrupted signals to estimate $\frac{m}{I}$ following the formulation in Equation 26.

Table 1 shows the identification results for the square and ellipse, for different values of the signal to noise ratio. The first column details the mean error and standard deviation in predicting the value of $\frac{I}{m}$, the second column denotes the percent error and the final column denotes the signal to noise ratio. We see good agreement between the predicted and true parameter with low levels of noise and a steady deterioration of prediction as noise is increased. One particularly damaging deterioration that noise produces is the modification of the contact geometry of the problem, of contact Jacobian. Poor evaluation of these variables results in poor behavior identifiability.

The proposed algorithm can also estimate contact forces. We show an example with the rimless wheel, in this case assuming we know its mass m, since we have already determined that in the absence of external forces, these are coupled. Figure 11 shows the estimated profile of the contact normal for an example where where the rimless wheel happens to roll without sliding. the plot shows impacts from three different spokes.

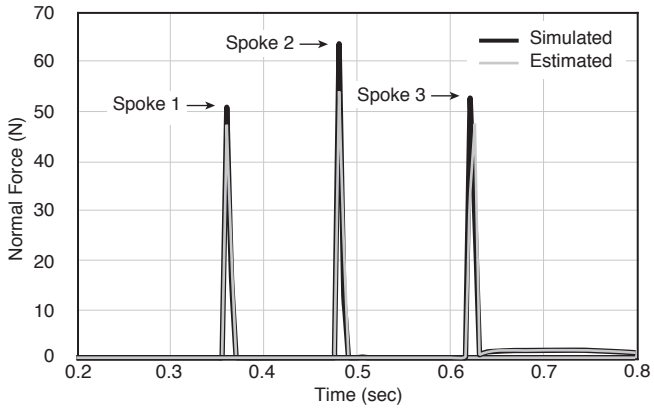

Figure 11: Estimation of the normal force during an impact of the rimless wheel with the ground from simulated data. Note that three different spokes undergo impact, so we show the reconstructed profiles for those three spokes.

5.4 Results from Experimental Data

In this section, we validate the proposed identification scheme with real data. To do so, we constructed the experimental setup in Figure 12, in likeness to the simulation environment used in the section above.

The *dropping arena* is constructed with two very flat sheets of glass with support spacers to constraint the motion of a falling object in the vertical plane. The objects are 3D printed in hard plastic, with shapes of a square of side-length 70 mms and of an ellipse with major and minor axis lengths of 70 and 50 mms. We track the position of the objects with a Vicon motion tracking system at 250Hz which proved accurate enough to extract velocity estimates by low-pass filtering and differentiation. To collect ground truth measurements of force we use an ATI Gamma 6-axis force torque sensor with 1000 Hz sampling rate. For each drop experiment we considered the first 3 bounces, which are extracted automatically using the impact signature captured by the F/T sensor. Figure 13 shows an example of such a trajectory.

For the validation, we use the data from a total of 280 drop tests to estimate the ratio of mass to inertia of the objects, as well as the peak contact forces at contact. For the case of the ellipse, the ratio of mass to inertia was estimated as 587 m^2 with a standard deviation of 27.6, while the real value is 535 m^2. The mean error in peak contact force estimation was -12.12 N with a standard deviation of 31.59 N, there the average magnitude of the peak force was in the order of 135 N.

Figure 14 shows an example of contact force estimation. The ellipse is shown as it comes into contact with the surface, and the plot compares the estimated ground reaction force with the profile captured by the force-torque sensor. Note that the contact force shows oscillations post impact. This is due to vibrations induced on the ground after the first impact. To avoid their effects, we focus this analysis on estimate the timing and magnitude of the first impact.

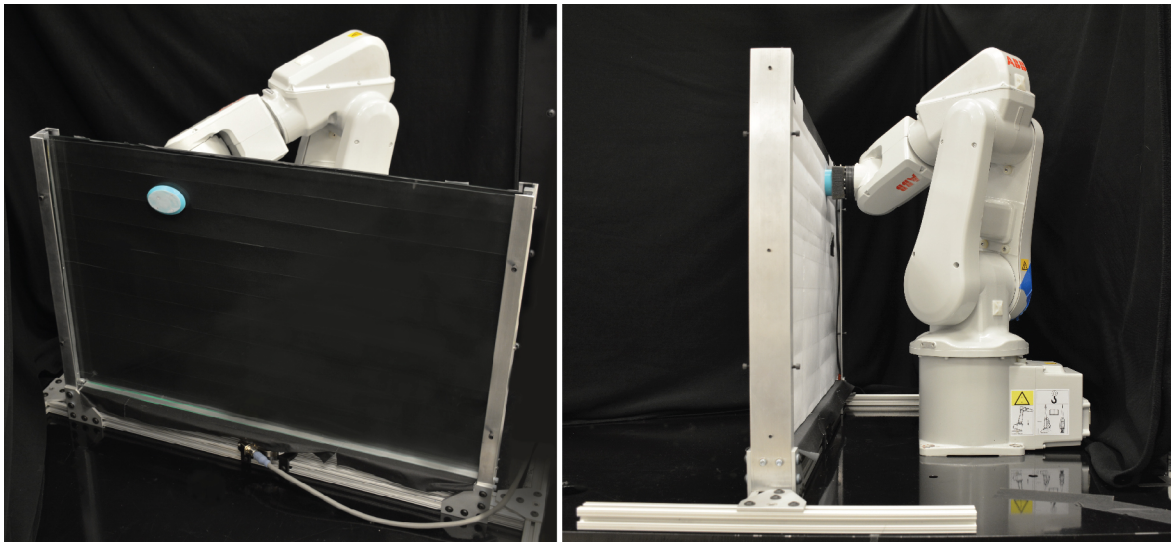

Figure 12: Experimental dropping setup. A six axis industrial robot latches magnetically on a part, gives it some initial velocity and orientation, and drops it. A motion capture system and a F/T sensor capture the falling motion at high frequency.

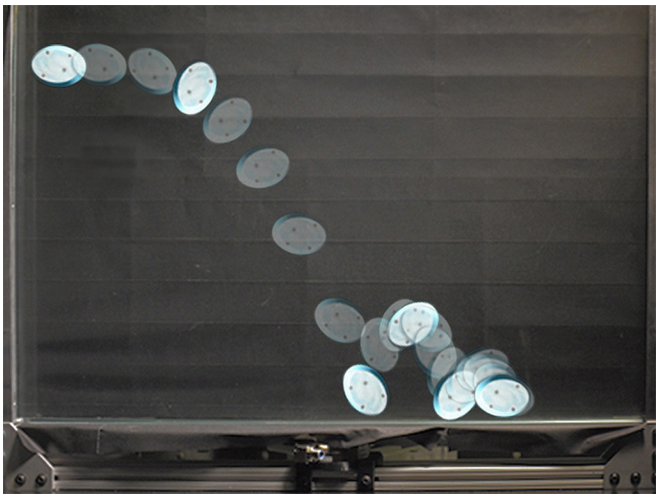

Figure 13: Example of a falling trajectory of a planar ellipse in the experimental dropping arena. The figure shows a sub-sampled trajectory recorded by the motion tracking system.

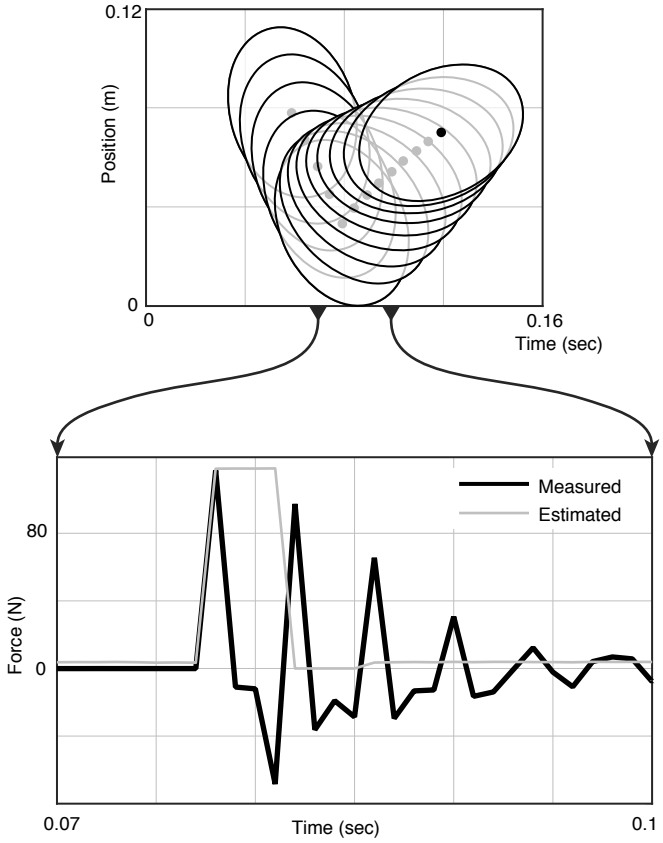

Figure 14: Reconstruction of the contact force for a impact of an ellipse. Note the oscillations of the measurements of the real force in the experimental setup. This is due to the vibrations induced after the first impact. It is a nuisance, so we focus on the ability of the algorithm to estimate the timing and magnitude of the first impact.

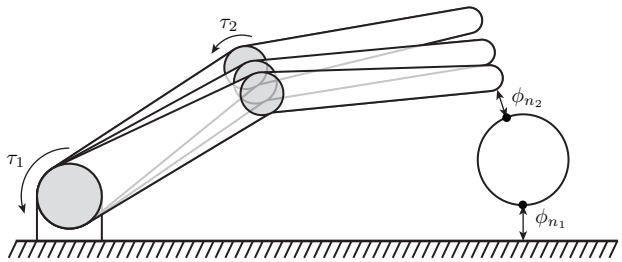

Figure 15: Schematic of the frictional interaction between a two-link manipulator, a disk, and the ground. In this case we have two simultaneous contacts, which we need to model with their correspondent rigid-body constraints, yielding, for example, two separate distances to contact ϕ_{n_1} and ϕ_{n_2}.

6 Identification for Multi-Body Interactions

In this section we demonstrate the application of the technique to a multi-body, multi-contact problem. Figure 15 shows a two link manipulator pushing a disk resting on flat ground. During the motion the disk makes and breaks contact with both the manipulator and the environment. Initially manipulator and disk are not in contact and the disk starts to drop from a height, subsequently the two link manipulator makes contact with the disk and pushes the disk against the ground, the disk begins to roll and slides its way out of the wedge formed by the manipulator and ground.

The system has a total of five degrees of freedom (two rotational joints of the manipulator and the position and orientation of the disk). Jointly with their velocities, these variables make for a 10-dimensional state space. We assume a maximum of 2 possible contact pairs at any given instant, the manipulator-ball pair and the ball-ground pair, and for each pair there are the associated normal and tangential contact forces in the contact frame, as well as their corresponding complementarity constraints. The control inputs are the joint torques of the manipulator, and everything is under the influence of a vertical gravitational field.

We adopt the formulation in Equation 18 and assuming a window length of m, the total number of parameters to estimate is $4m + 3 + 2$ where there are $2m$ forces per contact pair, 3 base inertial parameters of the two-link manipulator and 2 base inertial parameters of the ball. Note that the number of parameters to optimize grows linearly with the length of the window and there will be an additional $2m$ per any new contact pair.

To simulate the experiment we initialize the manipulator and disk in a configuration similar to Figure 15 and apply pre-determined torque profiles to the two-link manipulator. We log the resulting states and contact forces generated. Next we use the recorded configurations and torque profiles as inputs to Equation 18 along with the complementarity constraints to estimate the contact forces and base inertial parameters. Figure 16 shows estimated contact forces in the three directions between the disk and the manipulator overlaid with the simulated values.

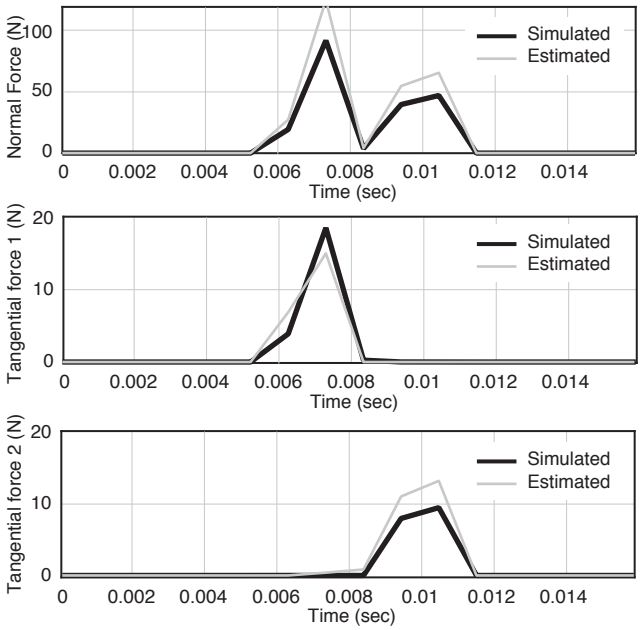

Figure 16: Estimation of the normal force c_n and two tangential forces $c_{t,1}$, $c_{t,2}$ during the brief interaction between the manipualtor and disk in Figure 15.

7 Practical Considerations

Practical implementation and uncertainty in measurements create interesting challenges. In this section we discuss some important details to consider when applying the approach outlined by this work.

7.1 Measurement Noise and Hard Constraints

The model we use in this paper for contact resolution assumes rigid contact. This yields several hard constraints that take the form of equality constraints in the optimization problem. Even if the objects and environment we use were to be perfectly rigid, sensor noise makes the observations violate those constraints. For example, it is often the case that objects slightly penetrate the ground, or that contact forces act at a sight distance from the ground, as shown in Figure 17. As a consequence, imposing the complementarity constraints on to the observed data proves challenging.

Ideally, one would want to do simultaneous state estimation and system identification, to reduce sensor noise. However, that is an important but complex topic for future work. In this work, we considered two possible solutions to alleviate this issue. The first is to employ a projection algorithm that at the time of contact imposes that objects be on the contact manifold. The second approach is to relax the strict equality and allow a slack proportional to the uncertainty in measurements.

The implementation of the first approach requires knowledge or detection of contact events which may be difficult, and the second approach allows for application of force at a distance, but the magnitude of such a force will be small. In our implementation we used the projection

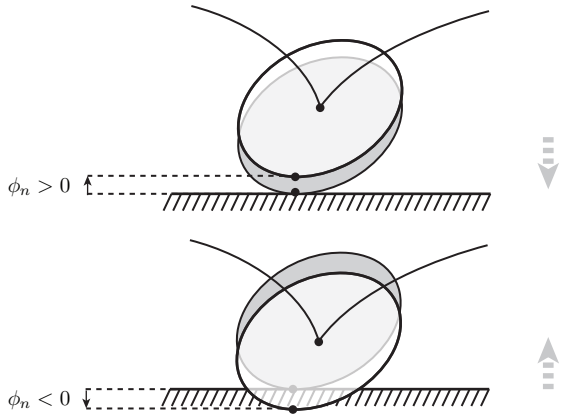

Figure 17: Noise in the pose measurement can lead to impacts happening in configurations that do not lie on the contact manifold. The image shows an example were an ellipse is projected (top) down or (bottom) up to satisfy the constraints of rigid contacts.

approach due to accurate knowledge of the ground elevation and relative high accuracy of sensors.

7.2 Sample Rate Variation across Sensors

Force sensors and joint encoders usually sample at a higher frequency than tracking/vision hardware. Our approach, however, assumes that during a window, sensor data is uniformly sampled and synched. In the event that sensor data is not uniformly sampled it is the authors experience that interpolation of the lower sample rate sensors works better than downsampling of faster sensors. This avoids throwing fine detail information that might be present in the high frame rate sensors, which is of special relevance for detecting contact events.

7.3 Persistence of Excitation

Persistence of excitation is a common consideration made when estimating parameters and variables in the context of system identification [21]. It quantifies how much a signal "excites" the dynamic modes of a system. We can build some intuition for this concept by considering again the Duffing oscillator discussed in Section 4.1:

$$m\ddot{x} + c\dot{x} + k_1 x + k_2 x^3 = a\cos(\omega)$$

If the amplitude and frequency of the excitation signal are both small, then the cubic stiffness term has very little effect on the output response of the oscillator and so estimates of the stiffness parameter k_2 will be poor. More formally, consider the class of systems that are linear in parameters $\boldsymbol{f}(t) = \boldsymbol{Y}(t)\boldsymbol{\theta}$, where $\boldsymbol{\theta}$ is the unknown parameter vector, $\boldsymbol{Y}$ is the known state dependant regressor matrix and $\boldsymbol{f}$ is a pseudo output vector. The persistence of excitation criteria requires that:

$$\alpha\mathbb{I} \leq \frac{1}{T}\int_{t}^{t+t_{obs}} \boldsymbol{Y}(\tau)^T \boldsymbol{Y}(\tau) d\tau$$

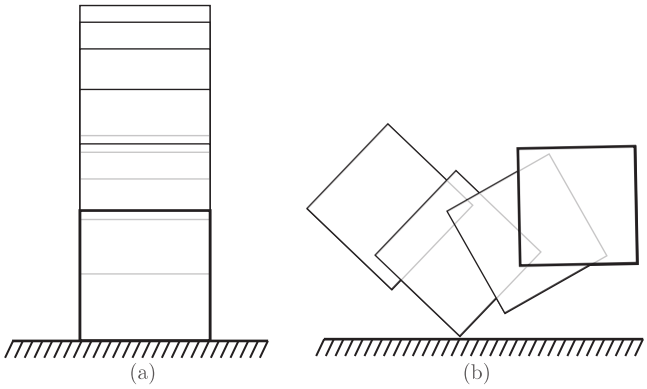

Figure 18: Example of (a) non-rich and (b) rich excitations for a bouncing square. The case of a vertical impact is indistinguishable from a point contact and hence it cannot possibly give information about the angular inertia of the object. The geometry of contact, and the corresponding regressor matrix $\boldsymbol{Y}$ is not full rank.

for the observed trajectories to be informative of the parameters to identify. The parameter α is a chosen positive scalar and $\mathbb{I}$ denotes the identity matrix. Intuitively, this criteria quantifies the positive-definiteness of the matrix $\boldsymbol{Y}(t)^T\boldsymbol{Y}(t)$ over the window of observation of length t_{obs}. Loosely put, the importance of the positive definiteness of this matrix is due to the inversion it undergoes in estimating the parameters over the time period.

Regarding the formulated nonlinear optimization Equation 18 the persistence of excitation criteria sets conditions on the Y and J_c matrices respectively. To be more illustrative, rather informally we write:

$$\left[Y(q^{k+1}, v^k, v^{k+1}, h) - J_c(q^{k+1})^T\right] \begin{bmatrix}\theta \\ c\end{bmatrix} = F^k_{\text{ext}}$$

$$\begin{bmatrix}\theta \\ c\end{bmatrix} = \left[Y(q^{k+1}, v^k, v^{k+1}, h) - J_c(q^{k+1})^T\right]^\dagger F^k_{\text{ext}}$$

The pseudo inverse of the regressor matrix is well posed when the criteria for persistent excitation of the signals is satisfied. Figure 18 shows an intuitive example, the contact of a square against a flat surface. In the left image the square lands perfectly on one side whereas on the right it lands at an angle. The left square will continue to bounce up and down vertically without ever rotating, implying no information can be deduced regarding its rotational inertia—in fact it cannot be distinguished from a point particle. The square on the right rotates with various angular velocities as it bounces, which provides information regarding its rotational inertia, so the excitation can be considered rich.

7.4 Rigidity of Interactions

The LCP formulation for contact resolution used in this paper assumes perfectly rigid bodies. In practice, bodies are not perfectly rigid, which means that velocities will not vary instantaneously, but rather will be modulated by the compliance-deformation of the materials. The formulation we presented is not adequate for systems that exhibit considerable compliance

during contact. The contact model would need to be augmented to incorporate deformation, which is an interesting line of research for future work.

8 Conclusions and Future Work

In this paper we study the problem of estimating contact forces and inertial parameters of systems of rigid bodies undergoing planar frictional contact. We formulate the estimation as a nonlinear optimization problem, where the different contact modes, i.e. contact vs. no-contact and sticking vs. slipping, can effectively and compactly be written as complementarity conditions. We discuss the identifiability and identification of parameters and forces for systems with and without the presence of external forces. We provide analysis and experimental demonstration with simulated and real experiments for three simple systems: a free falling rigid body, a rolling/slipping rimless wheel, and a manipulator pushing a disk. We finish the paper with a discussion of practical considerations for the implementation of these algorithms, issues with non-rigid contacts, and criteria for persistence of excitation.

We would like to note that the key premise upon which the approach is formulated is rigid body contact. While this may constitute a large set of systems of interest in robotics, it is by no means all inclusive. There are important classes of systems that exhibit significant compliance during contact. We are interested in generalizing the approach presented here to more complex contact models that incorporate compliance and deformation. Further, note that the contact resolution technique we use (LCP) is just one of several models available. In the future we plan to evaluate the performance of various models such as [2, 11].

The focus of this paper is on estimating contact forces and inertial parameters, and we implicitly assumed that the geometry of contact, i.e., shapes and poses, are known. Uncertainty in the geometry of the problem however presents a difficult challenge with important implications which is an exciting direction to explore.

Acknowledgments

We sincerely wish to thank Elliot Donlon for his help in the design and fabrication of the dropping arena, and the rest of the MCube Lab at MIT for all support and feedback. We also want to thank the extended and insightful feedback from the reviewers that did such a careful and lengthy evaluation of this paper. This work was supported by the National Science Foundation awards [NSF-IIS-1427050] and [NSF- IIS-1551535] through the National Robotics Initiative.

Appendix A Single Rigid Body Sliding Contact Mode:

Expressions for the terms in Equation 20 are given by:

$$
\begin{aligned}
M^{-1} &= \begin{bmatrix} \frac{1}{m} & 0 & 0 \\ 0 & \frac{1}{m} & 0 \\ 0 & 0 & \frac{1}{m} \end{bmatrix} \\
G(q^k) &= \begin{bmatrix} 0 \\ mg \\ 0 \end{bmatrix} \\
F^k_{\text{ext}} &= \begin{bmatrix} F^k_x & F^k_y & F^k_\theta \end{bmatrix}^T \\
\tilde{\omega}^k &= \begin{bmatrix} 0 & -\dot{\theta}^k & 0 \\ \dot{\theta}^k & 0 & 0 \\ 0 & 0 & 0 \end{bmatrix} \\
R^k &= \begin{bmatrix} \cos\theta^k & -\sin\theta^k & 0 \\ \sin\theta^k & \cos\theta^k & 0 \\ 0 & 0 & 1 \end{bmatrix} \\
C(q^k, v^k) &= \begin{bmatrix} 0 \\ 0 \\ \tilde{\omega} R I_0 R^T \omega \end{bmatrix} = \begin{bmatrix} 0 \\ 0 \\ 0 \end{bmatrix}
\end{aligned} \tag{33}
$$

The expressions for the linear mapping for the sliding mode are given by:

$$
\boldsymbol{f} = \begin{bmatrix} \begin{bmatrix} v_x^{k+1} - v_x^k \\ v_y^{k+1} - v_y^k + hg \end{bmatrix} - \begin{bmatrix} \mu \\ 1 \end{bmatrix} \left(v_y^k + v_\theta^k J_y^k - hg \right) \\ v_\theta^{k+1} - v_\theta^k \end{bmatrix} \tag{34}
$$

$$
\begin{aligned}
\boldsymbol{y}_1 &= \begin{bmatrix} hJ_y^k F_\theta^k \begin{bmatrix} \mu \\ 1 \end{bmatrix} + \left({J_y^k}^2 + \mu J_x^k J_y^k \right) h \begin{bmatrix} F_x^k \\ F_y^k \end{bmatrix} \\ \left(J_y^k + \mu J_x^k \right) h F_y^k + h F_\theta^k \end{bmatrix} \\
\boldsymbol{y}_2 &= \begin{bmatrix} hF_y^k \mu + hF_x^k \\ hF_y^k \\ 0 \end{bmatrix} \\
\boldsymbol{y}_3 &= \left(J_y^k + \mu J_x^k \right) \begin{bmatrix} -J_y^k \begin{bmatrix} v_x^{k+1} - v_x^k \\ v_y^{k+1} - v_y^k + hg \end{bmatrix} \\ v_y^k + v_\theta^k J_y^k - hg - \left(v_\theta^{k+1} - v_\theta^k \right) J_y^k \end{bmatrix} \\
\boldsymbol{y}_4 &= \begin{bmatrix} 0 \\ 0 \\ \left(J_y - \mu J_x \right) h J_y \tau \end{bmatrix}
\end{aligned} \tag{35}
$$

Appendix B Single Rigid Body Sticking Contact Mode:

The expressions for the linear mapping for the sticking mode are given by:

$$\begin{aligned} \boldsymbol{f} &= \begin{bmatrix} v_x^{k+1} + v_\theta^k J_x^k \\ v_y^{k+1} + v_\theta^k J_y^k \\ v_\theta^{k+1} - v_\theta^k \end{bmatrix} \\ \boldsymbol{Y} &= \begin{bmatrix} \boldsymbol{y}_1 & \boldsymbol{y}_2 & \boldsymbol{y}_3 & \boldsymbol{y}_4 \end{bmatrix} \end{aligned} \tag{36}$$

with:

$$\begin{aligned} \boldsymbol{y}_1 &= \begin{bmatrix} -\left({J_y^k}^2 + {J_x^k}^2\right) v_x^{k+1} + {J_x^k}^2 v_x^k + J_x^k J_y^k \left(v_y^k - hg\right) \\ -\left({J_y^k}^2 + {J_x^k}^2\right) v_y^{k+1} + J_x^k J_y^k v_x^k + {J_y^k}^2 \left(v_y^k - hg\right) \\ -\left({J_y^k}^2 + {J_x^k}^2\right) v_\theta^{k+1} - J_x^k v_x^k - J_y^k \left(v_y^k - hg\right) \end{bmatrix} \\ \boldsymbol{y}_2 &= h \begin{bmatrix} F_x^k \\ F_y^k \\ 0 \end{bmatrix} \\ \boldsymbol{y}_3 &= h \begin{bmatrix} -F_x^k {J_y^k}^2 + F_y^k J_x^k J_y^k - J_x^k F_\theta^k \\ F_x^k J_x^k J_y^k - {J_x^k}^2 F_y^k - J_y^k F_\theta^k \\ -F_x^k J_x^k - F_y^k J_y^k + F_\theta \end{bmatrix} \\ \boldsymbol{y}_4 &= \begin{bmatrix} 0 \\ 0 \\ -({J_x^k}^2 + {J_y^k}^2) h F_\theta^k \end{bmatrix} \end{aligned} \tag{37}$$

(38)

References

[1] M. Anitescu and F. A. Potra. Formulating Dynamic Multi-Rigid-Body Contact Problems with Friction as Solvable Linear Complementarity Problems. *Nonlinear Dynamics*, 14(3): 231–247, 1997.

[2] M. Anitescu and F. A. Potra. A time-stepping method for stiff multibody dynamics with contact and friction. *International Journal for Numerical Methods in Engineering*, 55(7): 753–784, Nov. 2002.

[3] C. G. Atkeson. State estimation of a walking humanoid robot. In *IEEE/RSJ International Conference on Intelligent Robots and Systems (IROS)*, pages 3693–3699, 2012.

[4] K. Ayusawa, G. Venture, and Y. Nakamura. Identifiability and identification of inertial parameters using the underactuated base-link dynamics for legged multibody systems. *International Journal of Robotic Research*, 33(3):446–468, 2014. URL `http://dx.doi.org/10.1177/0278364913495932`.

[5] S. Barai and P. Pandey. Vibration Signature Analysis Using Artificial Neural Networks. *Journal of Computing in Civil Engineering*, 9(4):259–265, 1995.

[6] S. Boyd and L. Vandenberghe. *Convex optimization*. Cambridge university press, 2004.

[7] B. Brogliato, A. ten Dam, L. Paoli, F. Génot, and M. Abadie. Numerical simulation of finite dimensional multibody nonsmooth mechanical systems. *Applied Mechanics Reviews*, 55(2):107, 2002.

[8] N. Chavan Dafle and A. Rodriguez. Prehensile Pushing: In-hand Manipulation with Push-Primitives. In *IEEE/RSJ International Conference on Intelligent Robots and Systems (IROS)*, pages 6215 – 6222, 2015. URL `http://dx.doi.org/10.1109/IROS.2015.7354264`.

[9] R. W. Cottle, J.-S. Pang, and R. E. Stone. *The Linear Complementarity Problem*. Academic Press, 1992.

[10] A. De Luca and R. Mattone. Sensorless robot collision detection and hybrid force/motion control. In *IEEE International Conference on Robotics and Automation (ICRA)*, pages 999–1004, 2005. URL `http://dx.doi.org/10.1109/ROBOT.2005.1570247`.

[11] E. Drumwright and D. A. Shell. A robust and tractable contact model for dynamic robotic simulation. In *ACM symposium on Applied Computing*, pages 1176–1180. ACM, 2009.

[12] M. Erdmann. Observing pose and motion through contact. In *IEEE International Conference on Robotics and Automation (ICRA)*, volume 1, pages 723–729, 1998.

[13] N. Fazeli, R. Tedrake, and A. Rodriguez. Identifiability analysis of planar rigid-body frictional contact. In *International Symposium on Robotics Research (ISRR)*, 2015.

[14] M. Gautier and W. Khalil. On the identification of the inertial parameters of robots. In *IEEE Conference on Decision and Control*, pages 2264–2269, 1988.

[15] S. Goyal, A. Ruina, and J. Papadopoulos. Planar Sliding with Dry Friction Part 1 . Limit Surface and Moment Function. *Wear*, 143:307–330, 1991.

[16] F. Hogan and A. Rodriguez. Feedback Control of the Pusher-Slider System: A Story of Hybrid and Underactuated Contact Dynamics. In *Workshop on Algorithmic Foundation of Robotics (WAFR)*, 2016.

[17] P. Khosla and T. Kanade. Parameter identification of robot dynamics. In *IEEE Conference on Decision and Control*, pages 1754–1760, 1985.

[18] R. Kolbert, N. Chavan Dafle, and A. Rodriguez. Experimental Validation of Contact Dynamics for In-Hand Manipulation. In *International Symposium on Experimental Robotics (ISER)*, 2016.

[19] S. Kolev and E. Todorov. Physically consistent state estimation and system identification for contacts. In *IEEE/RAS International Conference on Humanoid Robots (Humanoids)*, pages 1036–1043, 2015. URL `http://dx.doi.org/10.1109/HUMANOIDS.2015.7363481`.

[20] M. Koval, N. Pollard, and S. Srinivasa. Pose estimation for planar contact manipulation with manifold particle filters. *The International Journal of Robotics Research*, 7(34): 922–945, 2015.

[21] L. Ljung. *System Identification: Theory for the user*. Prentice Hall PTR, 1999.

[22] K. M. Lynch and M. T. Mason. Stable Pushing: Mechanics, Controllability, and Planning. *The International Journal of Robotics Research*, 15(6):533–556, Dec. 1996.

[23] L. Manuelli and R. Tedrake. Localizing External Contact Using Proprioceptive Sensors: The Contact Particle Filter. In *IEEE/RSJ International Conference on Intelligent Robots and Systems (IROS)*, 2016.

[24] J.-S. Pang and J. C. Trinkle. Complementarity Formulations and Existence of Solutions of Dynamic multi-Rigid-Body Contact Problems with Coulomb Friction. *Mathematical Programming*, 73(2):199–226, 1996.

[25] R. Platt and L. Kaelbling. Efficient planning in non-gaussian belief spaces and its application to robot grasping. *International Symposium on Robotics Research (ISRR)*, 2011.

[26] M. Posa, C. Cantu, and R. Tedrake. A direct method for trajectory optimization of rigid bodies through contact. *The International Journal of Robotics Research*, 33(1):69–81, Oct. 2013.

[27] A. Rodriguez, D. Bourne, M. Mason, and G. F. Rossano. Failure detection in assembly: Force signature analysis. In *IEEE International Conference on Automation Science and Engineering*, pages 210–215. IEEE, Aug. 2010.

[28] O. Salawu. Detection of structural damage through changes in frequency:A review. *Engineering Structures*, 19(9):718–723, 1997.

[29] J.-J. E. Slotine. On the Adaptive Control of Robot Manipulators. *The International Journal of Robotics Research*, 6(3):49–59, 1987.

[30] D. Stewart and J. C. Trinkle. An Implicit Time-Stepping Scheme for Rigid Body Dynamics with Inelastic Collisions and Coulomb Friction. *International Journal for Numerical Methods in Engineering*, 39(15):2673–2691, 1996.

[31] D. E. Stewart. Rigid-Body Dynamics with Friction and Impact. *SIAM Review*, 42(1): 3–39, Jan. 2000.

[32] D. Tax, A. Ypma, and R. Duin. Support Vector Data Description Applied to Machine Vibration Analysis. In *5th Annual Conference of the Advanced School for Computing and Imaging*, pages 398–405, 1999.

[33] A. Willsky. A Survey of Design Methods for Failure Detection in Dynamic Systems. *Automatica*, 12(6):601–611, 1976.

[34] K.-T. Yu, J. Leonard, and A. Rodriguez. Shape and Pose Recovery from Planar Pushing. In *IEEE/RSJ International Conference on Intelligent Robots and Systems (IROS)*, pages 1208 – 1215, 2015. URL `http://dx.doi.org/10.1109/IROS.2015.7353523`.

[35] K.-T. Yu, M. Bauza, N. Fazeli, and A. Rodriguez. More than a Million Ways to be Pushed. A High-Fidelity Experimental Data Set of Planar Pushing. In *IEEE/RSJ International Conference on Intelligent Robots and Systems (IROS)*, 2016. URL `https://arxiv.org/abs/1604.04038`.

[36] L. Zhang and J. C. Trinkle. The application of particle filtering to grasping acquisition with visual occlusion and tactile sensing. In *IEEE International Conference on Robotics and Automation (ICRA)*, pages 3805–3812, 2012.

[37] L. Zhang, S. Lyu, and J. Trinkle. A dynamic bayesian approach to real-time estimation and filtering in grasp acquisition. In *IEEE International Conference on Robotics and Automation (ICRA)*, pages 85–92, 2013. URL `http://dx.doi.org/10.1109/ICRA.2013.6630560`.

[38] J. Zhou, R. Paolini, J. A. Bagnell, and M. T. Mason. A convex polynomial force-motion model for planar sliding: Identification and application. In *IEEE International Conference on Robotics and Automation (ICRA)*, 2016.